The Effect of Iron Bearing Minerals on Surfactant Adsorption in Chemical Enhanced Oil Recovery Applications

A Thesis

Presented to

The Faculty of the Department of Petroleum Engineering

University of Houston

In Partial Fulfillment

of the Requirements for the Degree

Master of Science

In Petroleum Engineering

By

Travis H. Comer

May 2017

The Effect of Iron Bearing Minerals on Surfactant Adsorption in Chemical Enhanced Oil Recovery Applications

_____

Travis H. Comer

Approved:

_____

Chair of the Committee
Dr. Konstantinos Kostarelos, Associate Professor
Department of Petroleum Engineering

Committee Members:

_____

Dr. Michael T. Myers, Associate Professor
Department of Petroleum Engineering

_____

Dr. Dimitrios G. Hatzignatiou, Professor
Department of Petroleum Engineering

_____

Dr. Sujeewa Palayangoda, Post Doctoral Fellow
Department of Petroleum Engineering

_____

Dr. Suresh K. Khator, Associate Dean
Cullen College of Engineering

_____

Dr. Mohamed Soliman,
Professor and Department Chair,
Department of Petroleum Engineering

Acknowledgements

This is dedicated to Michele, who has been a constant inspiration.

The Effect of Iron Bearing Minerals on Surfactant Adsorption in Chemical Enhanced Oil Recovery Applications

An Abstract

Of a

Thesis

Presented to

The Faculty of the Department of Petroleum Engineering

University of Houston

In partial fulfillment of the

Requirements for the Degree

Master of Science

In Petroleum Engineering

By

Travis H. Comer

May 2017

Abstract

A declining number of oil field discoveries has led to an increased interest in enhanced oil recovery (EOR) technologies to produce residual oil and gas deposits where natural pressure drives and artificial lift capabilities have been exhausted. A technique whereby surfactant solutions (surfactants, co-surfactants, polymers, etc.) are injected into reservoirs to reduce the interfacial tension, alter the wettability of the reservoir rocks and maintain a favorable endpoint mobility ratio can become economically viable. Surfactant losses due to adsorption is one of the major hurdles to be overcome with this EOR technique. The purpose of this research is to examine the effect of iron-bearing minerals within the reservoir on surfactant adsorption rates. To observe these effects, a series of dynamic adsorption measurements were conducted using sand packs containing varying amounts of iron-bearing minerals, including siderite and illite, using an internal olefin sulfonate surfactant. To measure the rate of adsorption, iron and surfactant concentrations were monitored in the produced fluid. From the study, it was found that surfactant adsorption showed a proportional relation with the iron content within the clay. It also appeared that surfactant partitioning was proportional to the amount of clay present, regardless of iron content. This partitioning is likely due to a surfactant layering effect that occurs due to charge shielding.

Table of Contents

List of Figures

List of Tables

Chapter 1: Introduction

Chemical Enhanced Oil Recovery (cEOR) is an ever–important field of study as production of oil through primary and secondary means becomes more difficult due to decline in conventional oil field discoveries and a limit to the industry's technological capabilities of artificial lift and waterflooding. What separates cEOR from other tertiary recovery efforts is the use of a mixture of surfactants, co-solvents, and polymers to reduce the interfacial tension that exists between residual oil and brine within oil reservoirs. The surfactant molecule interacts with brine and oil to form a microemulsion phase that allows for oil mobility and an increase in oil production where primary and secondary (waterflooding) efforts begin to yield minimal returns.

Surfactant molecules often contain positively– or negatively–charged groups that lead to the formation of the microemulsion phase, however, the molecules are also subject to interaction with the rock matrix within the reservoir. Often this interaction is manifested as adsorption of the surfactant molecules onto the rock. Since an economic concern in the application of surfactant enhanced oil recovery efforts is the expense of the chemicals, as well as the reliability of the formulations to form the microemulsion phase under reservoir conditions, adsorption of surfactant affects the formulation chemistry and would result in a larger surfactant injection requirement and a larger production cost.

The aim of this work is to observe, qualify, and quantify the nature of this interaction as adsorption of an anionic (negatively–charged) surfactant molecule on the surfaces of positively–charged ionic clays. The clay primarily used in this study is siderite (iron carbonate), with a comparison experiment performed with illite. The surfactant used is an anionic, internal olefin sulfonate.

To observe these effects, a set of synthetic sandstone cores were made that contained varying amounts of siderite or illite. It was important to use synthetic cores instead of field samples in order to remove any confounding effects that variances in porosity, permeability, particle size distribution, and heterogeneity may have on the adsorption results. This also allows a more precise knowledge of the amount of clay particles within the core, as they are mixed in and controlled during the core preparation procedure. After an injection of a reducing agent to ensure that the iron ions are in a low valence state (the state in which they exist *in-situ*), surfactant is injected and the effluent analyzed to quantify the adsorption.

This thesis contains reports on the adsorption values through a set of cores that contained 0, 2.5, 5, and 10 wt.% siderite. A core containing 10 wt.% illite was also used in the experimental set as a comparison. An effort to qualify the adsorption process by way of effluent analysis and other observations is also a part of this thesis.

Chapter 2: Background

To best contextualize the significance of this research, this chapter will serve to provide background surrounding the history and science of enhanced oil recovery, the role of surfactants and surfactant chemistry in chemical enhanced oil recovery, the cause and consequences of adsorption of surfactants within oil reservoirs, and the methods to model and analyze surfactant laboratory core flood experiments.

2.1: Enhanced Oil Recovery

The global demand for oil has been steadily increasing since its first discovery and use as an energy source in the late 19th century. The EIA predicts that energy consumption in the US alone will reach nearly 110 quadrillion BTUs (British Thermal Units) a year by 2040, with roughly a third of that demand satisfied by petroleum and other liquids. (EIA, 2016) Crude oil and petroleum derivatives also serve as important chemical feedstocks, which further increase oil's importance in current markets and economies. As a finite resource, oil discoveries will naturally become scarcer and the cost of extraction will trend upwards. **Figure 1** below shows a relationship between green field discoveries and oil demand from the past and forecast into the future. There is a significant decline in conventional field discoveries beginning in the late 1980s. Despite technological advancements that allow for higher efficiencies and greater production in conventional reservoirs, the consumption of oil produced through traditional methods begins to deviate from the forecast demand near 2010, as unconventional shale drilling techniques became more prolific.

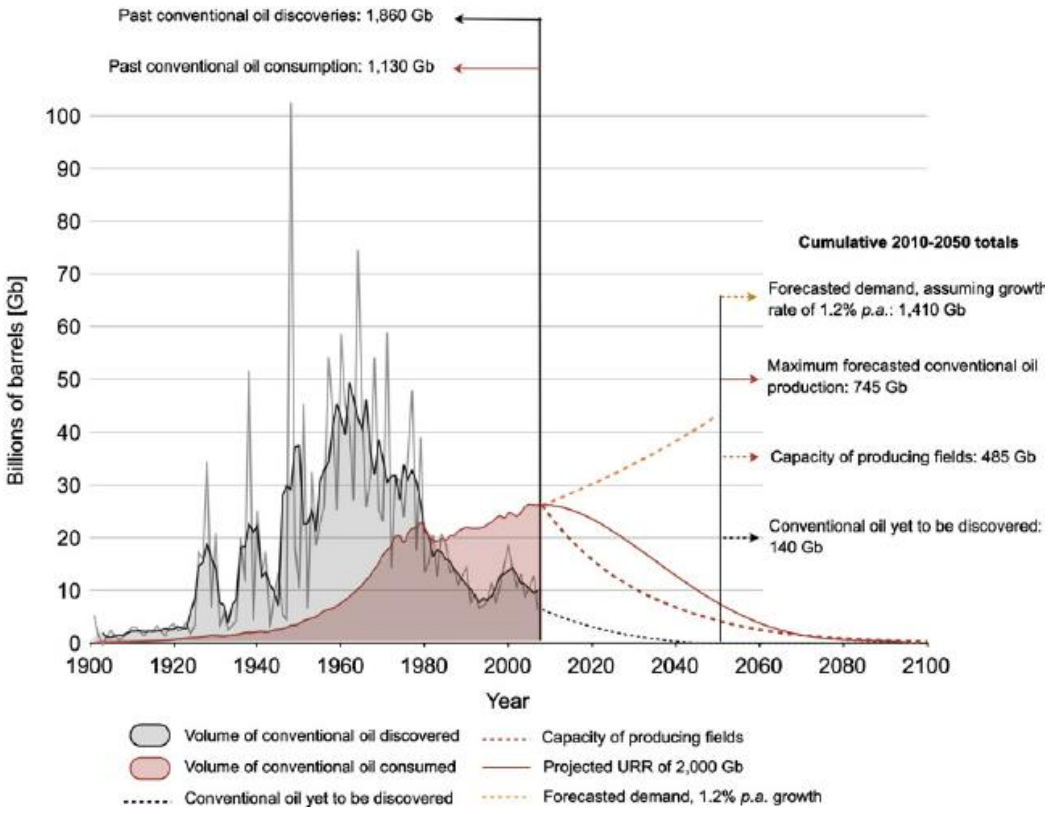

Figure 1: Annual backdated 2P conventional oil discovery, conventional oil consumption, and forecasted production and discovery (Owen *et al.*, 2010)

Since the rate of new field discoveries is declining, an intuitive solution to satisfy the ever–increasing global demand for fossil fuel, enhanced oil recovery solutions in the form of water, gas, and surfactant injection can help produce stranded oil from brown field reservoirs that have been depleted through traditional methods. Enhanced oil recovery, or EOR, will likely become a widely–used set of technologies to maximize the production of the world's reserves. This, coupled with other new drilling and production techniques such as horizontal wells, hydraulic fracturing, and shale/tight oil reserves exploitation, will soon make up a large percentage of overall oil production in the near future. To better appreciate the need for enhanced oil recovery, the following sub–

sections will include discussion surrounding the variances and terminology between primary, secondary, and tertiary oil recovery (EOR).

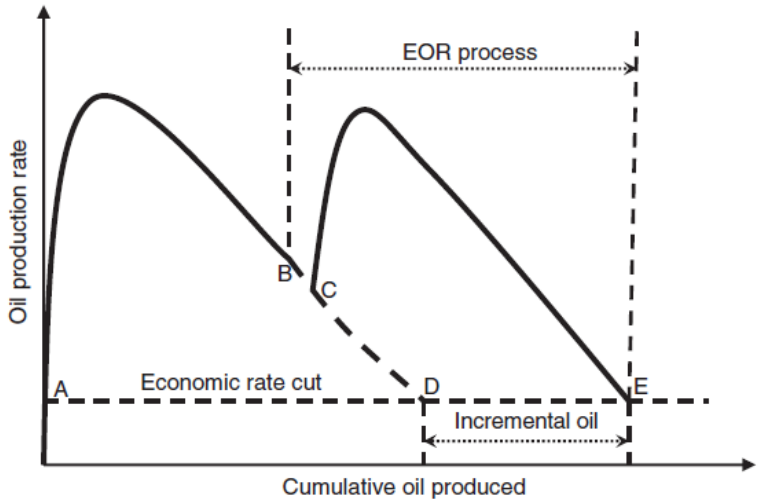

Figure 2: A general visualization of the rate improvements of EOR processes in declining wells. Point A to B represents the initial rate increase and decline, and points C to E shows the rate increase and decline from an EOR process. The difference between the cumulative oil produced at points E and D represent the marginal oil recovered due to EOR. (Sheng, 2015)

In **Figure 2**, a visual is provided demonstrating a possible rate and cumulative oil production over the periods of an EOR field exploitation project. These may not always be the ratios, nor sequence in which the techniques are employed, as those are dictated by the nature of the reservoir and economics involved in oil production. Considering this, the terms primary, secondary, and tertiary recovery can be considered slight misnomers. For example, it may be considered more economical to perform water or gas injection immediately after drilling rather than waiting for natural pressure drives to be depleted.

2.1.1: Primary Recovery

Primary oil recovery is the descriptor for production from reservoirs through natural means (pressure drives from aquifer, gas caps, solution gas, and gravity drainage). Though the oil recovered by natural pressure drive mechanisms will vary depending on

the geology, deposition, and fluid components, the amount produced can be between 5% and 25% of the original oil in place (abbreviated as OOIP). (Bantignies *et al.*, 1997) Sometimes, when natural pressure drives are depleted, wells can continue to produce in primary production with the aid of artificial lift technologies such as beam and electric submersible pumps (ESPs).

2.1.2: Secondary Recovery

Secondary recovery generally refers to the practice of waterflooding an oil reservoir. In most cases, waterflooding is a process used after production has been rendered uneconomical due to a lack of pressure drive. However, waterflooding can also be useful to maintain (or increase) reservoir pressure or speed-up recovery. In this technique for on-shore reservoirs, a pattern of injection wells is drilled (or producers are re-purposed) to inject water into a reservoir, sometimes with polymer to prevent channeling and early breakthrough. Waterflooding is also used in off-shore applications, though without pattern injection wells due to higher drilling costs. In this injection technique, water is used as a displacing agent that forces oil towards a production well. Its economic limit is that where the fraction of oil produced is too low to sustain the capital costs associated with the injection process and water disposal.

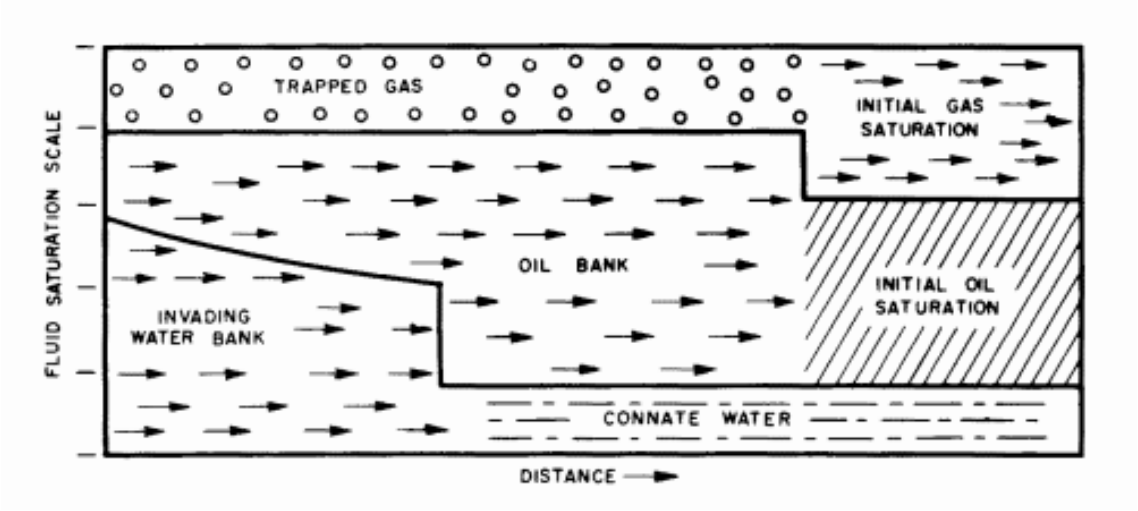

Figure 3: Saturation profile during a waterflood in a depleted reservoir with trapped gas is shown. As water is injected (left to right), the oil is displaced towards a producing well. (Wilhite, 1986)

Waterflooding has become standard practice for wells with naturally–declining production. Generally, a waterflooded field can yield 10% to 20% of the OOIP after recovery from primary production drives. (Bantignies *et al.*, 1997)

2.1.3: Tertiary Recovery

EOR, or tertiary recovery, is a descriptor for a set of oil production techniques that are often used to produce oil from reservoirs that have exhausted primary drives and where waterflooding yields uneconomical results. Often, this occurs as water has surrounded stranded 'ganglia' of oil forming a residual oil zone. This oil is trapped due largely as a result of the interfacial tension that exists between the water and hydrocarbon molecules.

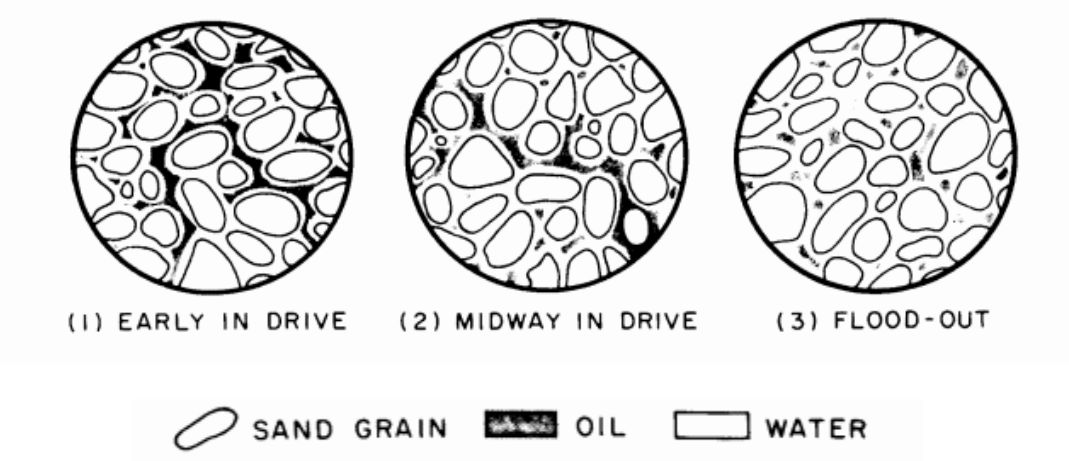

Figure 4: Fluid distribution during and after a waterflood in a water wet reservoir are shown. As the maturity of the waterflood project increases from left to right, the residual oil saturation decreases to a point where the low fraction of oil produced renders the effort uneconomical. (Wilhite, 1986)

Most often, tertiary recovery projects are operated by injecting fluids (CO_2, steam, surfactants, *etc.*) that alter oil properties to allow trapped oil to mobilize and travel within thee pore spaces of the reservoir towards a producing well. In surfactant flooding, the aim is to reduce the interfacial tension between the aqueous and organic phases.

2.2: Surfactant Chemical Injection

In surfactant chemical enhanced oil recovery, the agent that reduces the interfacial tension causing trapped or residual oil is a formulation consisting of surfactants, co–solvents, neutral salt materials, and polymers. Each of these components assist in the formation of a micellar structure of the surfactant and a microemulsion phase that recovers residual oil by forming an oil bank and drives the oil towards a producing well.

The appropriate formulation for each reservoir is found through meticulous study and experimentation with the reservoir fluids, both brine and oil. Co-solvents are alcohols that, when added, can prevent gels from forming when micelles coagulate; neutral salts are added to shield charges and ensure that thermodynamic equilibrium can

exist between the phases, and; polymers are added for mobility control to prevent channeling in potential anisotropic reservoirs and viscous fingering. (Sheng, 2011; Lake *et al.*, 2014)

2.2.1: Surfactant Chemistry

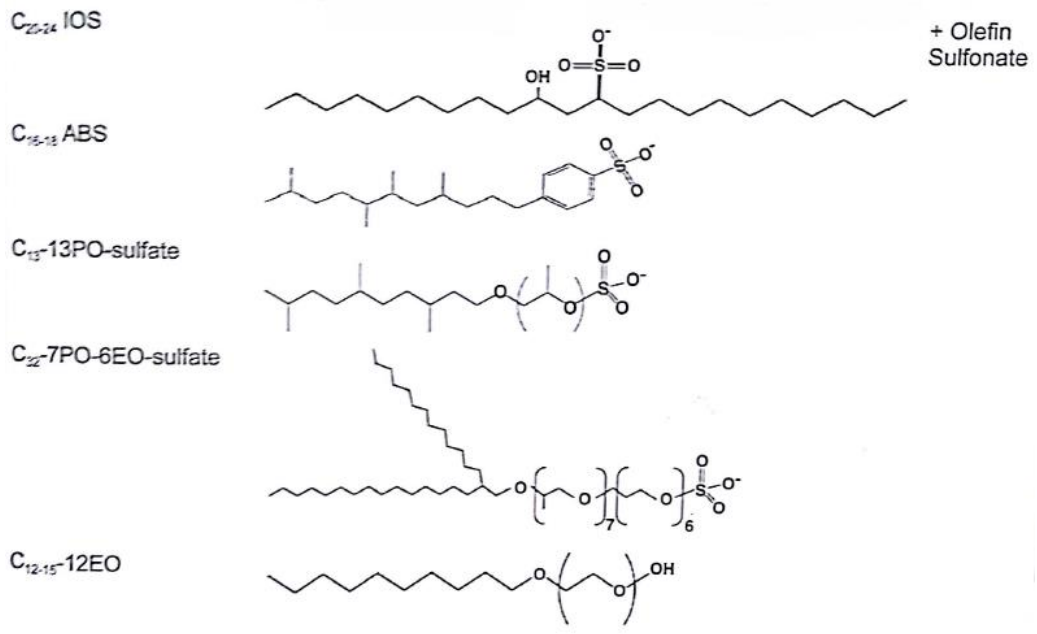

Figure 5: Examples of surfactant molecular structures (Lake *et al.*, 2014)

The amphoteric behavior of a surfactant molecule makes it ideal for reducing the interfacial tension between an aqueous and an organic phase. Surfactant molecules contain a hydrophobic moiety, which normally consists of a hydrocarbon chain of various lengths, and a hydrophilic moiety. The hydrophilic head group of the surfactant molecule can be positively charged, negatively charged, or neutral. In **Figure 5,** several surfactant molecule structures are shown, demonstrating the variety of combinations between charge, head groups, tail length, and other chemical components. The nature of the reservoir rock type and fluids dictate the best surfactant or surfactant combination to

maximize effective production. Generally, the use of surfactants to lower the interfacial tension between brine and crude oil within a reservoir with a fixed salinity and oil density requires extensive study and formulation. (Sheng, 2011) These formulations are essential in promoting the development of a microemulsion phase—a thermodynamically stable phase wherein both organic and aqueous phases reside. As a result, the interfacial tension between the phases is reduced to very low values that, in turn, allows the trapped oil to become mobilized and produced. This microemulsion phase can only occur when the concentration of surfactant surpasses the critical micelle concentration (CMC), a threshold above which surfactant monomers cannot exist in the solution begin to form micellar structures with any subsequent increase in concentration. It has been shown that retention of surfactant within a reservoir can alter the rock wettability in ways that make finding optimum formulations more complex. (ElMofty, 2012)

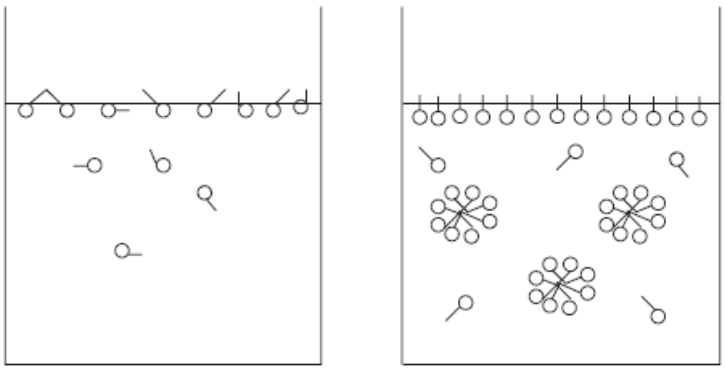

Figure 6: At low concentrations, surfactant molecules exist at monomers that adsorp to surfaces and interfaces due to there amphoteric nature (left). As their concentration is increased, Formation of micelles occurs as surfactant concentration is increased (right) . Above the CMC, the addition of surfactant results in only micelle formation. (from Sheng, 2011)

2.2.2: Interfacial Tension

At some point in the oil production process, oil is stranded in the form of small isolated droplets within the pore space of the reservoir rock. The oil saturation is termed *residual oil saturation*. When displacing resident fluid by an invading fluid, the dimensionless numbers describing the process are the capillary number, bond number, and the trapping number. (Jin, 1995) These are shown below as

$$N_C = Ca = (\mu U) / \sigma, \quad (1)$$

$$N_B = \frac{\Delta \rho g L^2}{\sigma}, \text{ and} \quad (2)$$

$$N_T = (N_C^2 - 2N_C N_B \sin(\alpha+\beta) + N_B^2)^{1/2} . \quad (3)$$

Equation 1 is a relation for calculating the capillary number, a function of viscosity, superficial velocity, and interfacial tension that are represented by the symbols μ, U, and σ, respectively. It is essentially the ratio of viscous forces compared to that of the interfacial tension acting on the interface of the phases within the reservoir. The symbol, N_B, in equation 2 represents the Bond number, is a dimensionless number comparing the buoyant forces acting to displace the resident phase and the capillary forces acting to trap the resident phase. In equation 3, the Trapping Number incorporates both the Bond Number and Capillary Number, and thus compares the forces acting to displace oil with the force acting to trap oil. Early work in EOR did not include the effect of buoyancy and reference the capillary number instead of the trapping number as shown below in **Figure 7**. The capillary desaturation curve shown in **Figure 7** can still be useful to understand the role of reduced IFT on oil recovery. Noting that the residual oil saturation remains constant as the capillary number is increased until reaching the critical capillary

number, where further increases in N_C result in mobilization of oil and complete recovery of trapped oil is possible. Thus, the goal of enhanced oil recovery techniques is to increase the capillary (or trapping number if we include the buoyancy effect) to a point at which the trapped oil is mobilized and produced.

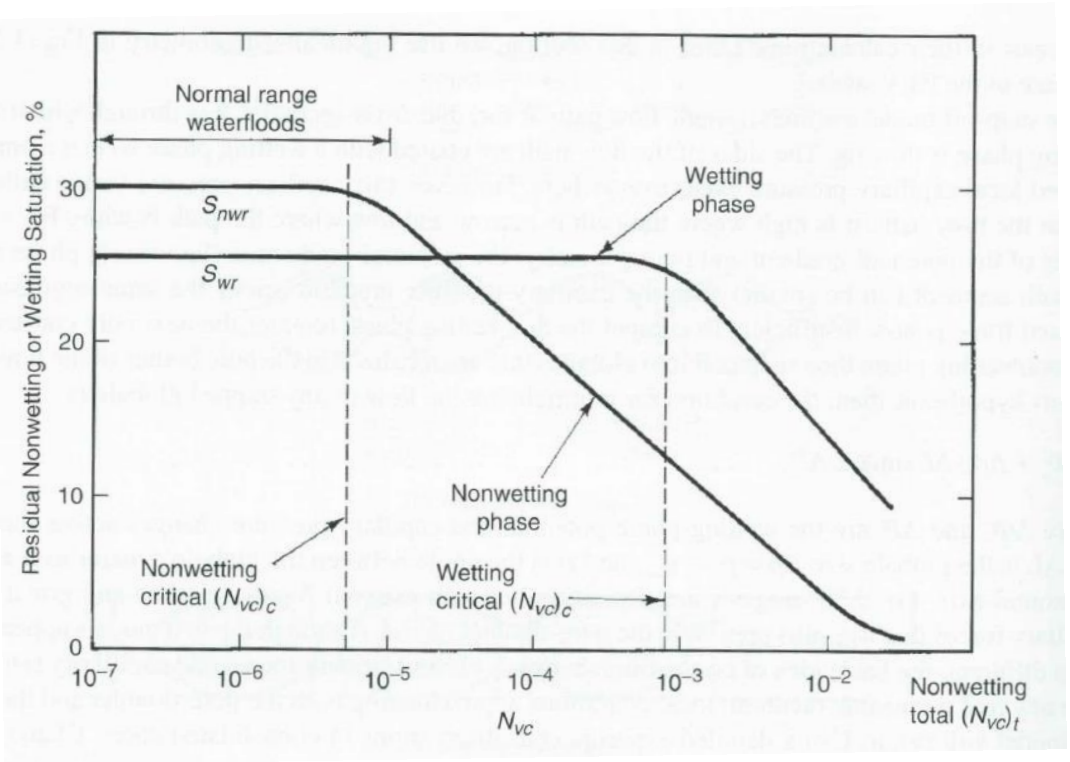

Figure 7: Capillary desaturation curves based on capillary number show the critical capillary numbers where residual oil saturation begins to decrease. (Lake *et al.*, 2014)

To increase the trapping number by way of increasing the displacing fluid's viscosity or velocity will not reach the critical value to mobilize the trapped oil. The only approach that can achieve a substantial increase in trapping number is by way of a significant decrease in IFT. This is best demonstrated by observing graphs such as that in

Figure 7, where it can be seen that N_C must increase by several orders of magnitude in order to reduce the residual oil saturation (y-axis) by any substantial margin.

2.2.3: Formation of Microemulsion

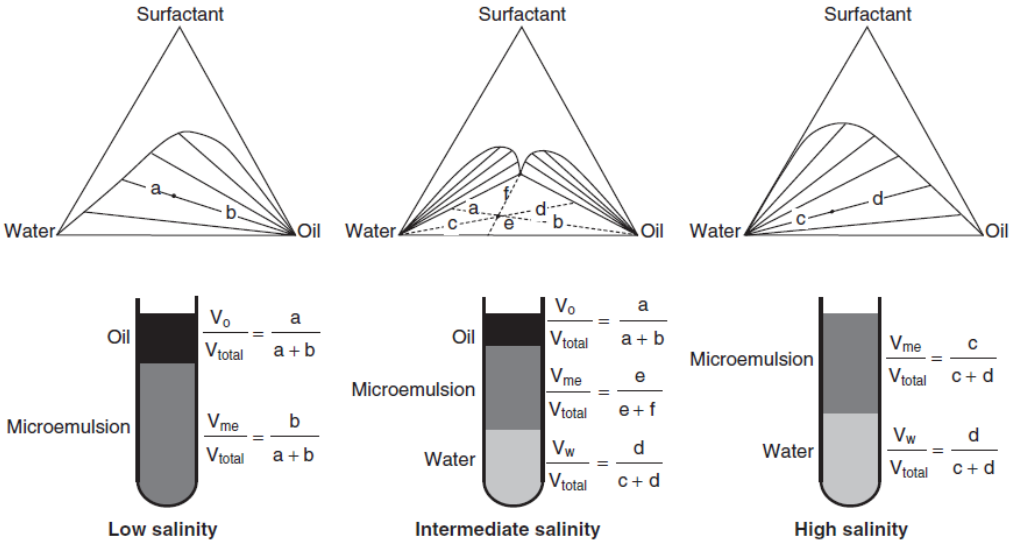

Figure 8: Ternary diagrams and related phase behavior for Type I, III, and II microemulsions shown from left to right (Sheng, 2011)

As mentioned in Section 2.2.1, the qualifying characteristic of surfactants for use in reducing IFT and use in EOR is its ability to form a microemulsion phase. Much research has been conducted regarding the careful formulation that is involved with selecting the surfactant, concentration, and salinity for given reservoir conditions and oil characteristics. **Figure 8** above provides a visual aid in understanding the phase behavior at various salinities. During the planning and laboratory phases of a potential surfactant enhanced oil recovery project, a surfactant is tested by mixing with brine and oil at various salinities, known as a salinity scan. There are at least three defined behavior 'types' that describe the microemulsion phase observed in the formulations. Winsor

Type I refers to a microemulsion wherein the surfactant micelles resides in the aqueous phase and oil is solubilized within the micelles of the aqueous phase with a slight reduction in IFT between the excess oil and the microemulsion. This occurs at at low salinity and is shown on the left of **Figure 8**. This microemulsion is also known as Type II(-), explained by the ternary on the left showing negatively–sloped tie lines in the phase envelope. Conversely, surfactant resides in the oil phase of a Winsor Type II microemulsion and the water is solubilized within micelles in the oil phase and the IFT between the excess water and microemulsion is slightly reduced. This microemulsion is also known as a Type II(+). A Type III microemulsion is one where oil and water are both solubilized within the microemulsion and the excess oil/excess water/microemulsion IFTs are significantly reduced. A Type III microemulsion is ideal for enhanced oil recovery, as it allows the formation of a pure oil bank that can be driven towards a producing well. (Lake *et al.*, 2014; Sheng, 2015)

2.3: Adsorption

The review of surfactant behavior and the role of microemulsion in enhanced oil recovery highlight the importance of the surfactant formulation consisting of surfactant, co-surfactant, co-solvent, electrolyte, and viscosifiers. If any of these components are altered before or during the injection process, the result could cause a project to become uneconomical. In this regard, the most significant concern would include the loss of surfactant (or other component) within the reservoir due to adsorption. As the concentration is lost, the microemulsion phase may be rendered ineffective or be lost as well. Thus, it is important to understand how rock properties affect surfactant adsorption so that we can anticipate and prepare for such occurrences in planning the project. It is

important to note that all components of the chemical formulation in cEOR could be adsorbed onto the reservoir rock or significantly affect adsorption, though this work concentrates solely on surfactant adsorption.

2.3.1: Mechanisms of Surfactant Adsorption

Surfactant adsorption is driven by a combination of: a) the interaction between the surfactant's head group and the solid surface and b) the hydrophobicity of the tail groups of the surfactant. The former is most relevant when observing the effects of iron bearing minerals on the adsorption mechanism. If the surface of the solid medium is hydrophilic or polar, adsorption occurs where the head group of the surfactant is attracted and attaches to the surface and the tail is either pointed inward towards the solution if the surfactant concentration is below the CMC, or inwards towards the micellar structure if the concentration is above the CMC. (Paria and Khilar, 2004)

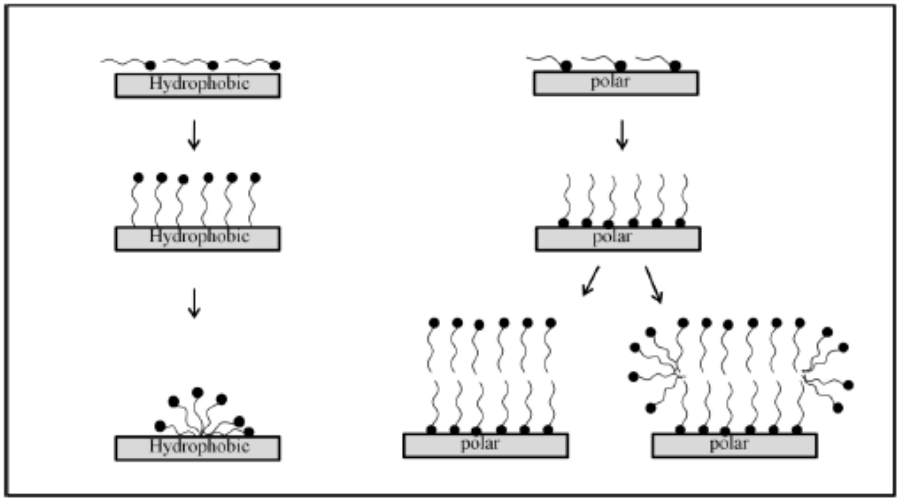

Figure 9: This illustration shows the ways surfactant molecules may adsorb to polar and hydrophobic surfaces. (Holmberg *et al*., 2002)

It has been observed that there are four adsorption mechanisms that vary depending upon the concentration of the surfactant in the solute. As shown in **Figure 9**,

at concentrations below CMC, the adsorption can be attributed to electrostatic interactions between the surfactant monomers and charged surfaces. Eventually, these monomers interact with each other to form hemicelles on the surface, and when the concentration is above the CMC, the micelles adsorb onto the surface in aggregate while not changing in adsorption density. (Zhang and Somasundaran, 2006) Any chemical factor that changes the strength of ionic charge can have a significant effect on the scale of retention of surfactants on solid surfaces, including the length of the hydrocarbon chain for the selected surfactant. (Somasundaran *et al.,* 1964) Recently, a model has been developed showing that surfactant retention in an oil reservoir can be a determined from temperature, pH, rock type, co-solvent concentration, average mobility ratio, and salinity. (Kamari *et al.,* 2015)

2.3.2: Surfactant Adsorption onto Iron Bearing Minerals

Iron bearing minerals tend to significantly affect surfactant retention due to the positive charge that iron ions have within the reservoir. This is especially true for anionic surfactants, where the negatively–charged head group will be attracted to these positive charges. Studies have been performed examining the adsorption of surfactants onto iron surfaces, specifically. In experiments designed to observe the effects that surfactants have on iron to examine corrosion inhibition, it was shown that the surfactant micelles tend to pack. This is despite a repulsion from similarly charged head groups. (Knag *et al.,* 2006) The layers form possibly as a result of charge shielding from the Fe^{2+} ions, along with the ions surrounding the micelles in the form of Na^{+} and Cl^{-}. (Knag *et al.,* 2004)

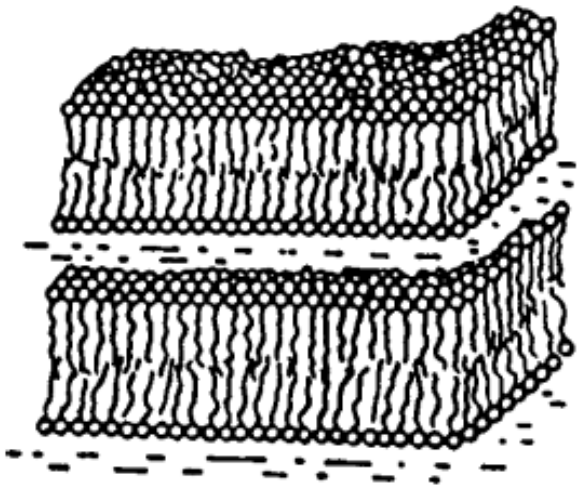

Figure 10: This sketch demonstrates of the packing of surfactants (and formation of liquid crystals) onto a charged surface as a result of charge shielding. The charges of the salt ions and those on the surface can shield the repulsion from the anionic surfactant head groups, allowing for a stacking to occur. (Knag e*t al.*, 2004)

In conditions where there are significant concentrations of ion charges (such as the salt and iron ions in this experimental set), the balance of these allow for the repulsion from the similarly charged head groups of the surfactant to be reduced and can result in these layered structures on a surface. In **Figure 10**, a sketch of surfactant micelles layered on a charged surface is depicted. These layers can form liquid crystals or gels, whose negative effects (such as pore throat blockage and constriction) can be mitigated through the inclusion of co-solvents in the surfactant formulation to help dissolve them.

2.3.3: Experimental Adsorption Simulation and Reducing Agents

In order to observe accurate (relative to field–observed values) adsorption of surfactant within a core containing iron–bearing minerals, it has been found that the core must be restored to its reduced state by reducing any oxidized iron components. In pilot tests of the Loudon field, a large discrepancy between the coreflood experimental retention and that of the field was observed. (Wang, 1993) Specifically, the coreflood

experiments overestimated the retention. Values observed in pilot field tests and experiments from Wang are compared in **Table 1** and **Table 2.**

Table 1: Observed and measured surfactant retention in Loudon pilot field (Wang, 1993)

	Surfactant retention (mg/g rock)		
Project	**Frontal Delay**	**Material Balance**	**Postpilot Cores**
First Ripley Pilot, 0.7 acre	NA	0.35	0.18
Second Ripley pilot, 0.7 acre	0.11	0.08	0.08
Expanded pilots, 40 and 80 acres	0.33	0.24	0.23

Table 2: Surfactant retention measured in Loudon field core plugs under various reduction scenarios (Wang, 1993)

Experiment	**Description**	**Surfactant retention (mg/g rock)**
1a	Conventional, 3-PV ME, 0.55 k_{ow} =290 md	0.55
1b	Conventional, 3-PV ME, 0.82 k_{ow} = 19 md	0.82
2a	Reduced by dithionite, 0.20 3-PV ME, k_{ow} =78 md	0.2
2b	Reduced by dithionite, 0.20 120-PV ME, k_{ow} =84 md	0.2
3a	Reduced by field brine, 0.20 3-PV field ME	0.2
3b	Reduced by field brine, 0.33 3-PV ME formulated with FB	0.33

In **Table 1**, the calculated adsorption values from three methods (frontal delay, material balance, and examination of post pilot cores) show a range of retention from 0.11 to 0.35 mg/g rock. **Table 2** shows that in experiments 1a and 1b, the retention is significantly overestimated. Subsequent experiments that use a reducing agent on the core all fall within the expected values based on the pilot projects.

The anaerobic *in situ* conditions that exist within the reservoir prevent the oxidation of iron ensuring inherent ionization and thus the mechanism by which this increased adsorption occurs. (Wang, 1993) To achieve this, a reducing agent in sodium dithionite (sodium hydrosulfite) is injected into the core prior to injection of the surfactant. Great care must also be taken to prevent oxygen from entering the experimental setup through the injected fluids and the components of the coreholder device. The chemical reaction that occurs to reduce the iron within the siderite is shown below.

$$S_2O_4^{2-} + 2Fe^{3+} + 2H_2O \xrightarrow{yields} 2SO_3^{2-} + 2Fe^{2+} + 4H^+ \quad (4)$$

During the experiment, the electric potential is measured (Eh) both before and after injection as an indication of the reduction-oxidation potential of the sodium dithionite solution to ensure complete reduction of the core. (Rajapaksha, 2014)

2.4: Experimental Analysis

For this work, the adsorption of the surfactant used in core flood experiments was determined by comparing the surfactant concentration of the injected fluid and to the effluent concentrations during the coreflood. Potentiometric titration was used to measure surfactant concentrations and a mass balance used to determine the surfactant

adsorption, while the method of moments was used to analyze the data for possible surfactant retardation.

2.4.1: Method of Moments

If the concentration history of a specific chemical species is known, the centroid of the curve can be found using the method of moments. For an injected fluid containing a conservative tracer (or surfactant that experiences no partitioning effects with neither a resident phase nor the reservoir material), calculating the first moment, $\bar{V}$, will also indicate the swept pore volume of the medium. The calculation is given by equations 5,

$$\bar{V} = \frac{\int_0^\infty V_j C_j (dV_j)}{\int_0^\infty C_j (dV_j)}, \tag{5}$$

that can be re-written for samples number j=1 to *n*,

$$\bar{V} = \frac{\sum_{j=1}^{n} V_j C_j (\Delta V_j)}{\sum_{j=1}^{n} V_j C_j} - \frac{1}{2} V_{slug}. \tag{6}$$

In equation 6, ΔV_j and C_j represent the sample volume and concentration of tracer in sample "*j*" produced at time V_j. In equation 6, the $\frac{1}{2} V_{slug}$ term is a correction that accounts for the practice of starting data collection at the start of injection rather than midway through the injection. If partitioning of the injected fluid is observed, then the method of moments will yield a calculated first moment that is higher than the measured pore volume that can be used to compute the retardation factor.

When a solute "*i*" is introduced to a mixture of two solvents that are immiscible, the solute will dissolve in both of these two phases. The concentration of the solute measured in each of these two phases depends on the affinity of the solute for each phase and will be the same when the measurement is repeated, provided the environmental

conditions are used. The ratio of the two concentrations is known as the *partition coefficient*. For example, the partition coefficient of solute (*i*) in phase (*n*) and phase (*j*) is defined as

$$K_i = \frac{C_{i,n}}{C_{i,j}}. \quad (7)$$

Thus, if a tracer is dissolved in water and pumped through a core where two phases exist (*e.g.*, oil and water), the tracer will partition between the two phases and, a delay in the production of the tracer is observed known as retardation. The retardation factor,

$$R_f = \frac{\bar{V}_2}{\bar{V}_1}, \quad (8)$$

where $\bar{V}$ is the first moment of the tracer and the subscript 2 represents the delayed (partitioning) tracer while the subscript 1 represents the conservative (non-partitioning) tracer. As mentioned earlier, partitioning phenomena can also be observed when tracers adsorb and then desorb from a solid surface, however, those that simply adsorb are not described this way.

2.4.2: Surfactant concentration measurements

There are several methods to measure surfactant concentration. One of these methods relies on titration. In general, the concept of titration involves using a titrant that interacts with the solute in a solution. An endpoint is determined based on the results of intermittent addition of the titrant into the solution.

In potentiometric titration for anionic surfactants, an electric probe measures the electric potential in a solution while measured drops of hyamine titrant is added. The electrode, itself, is a specially manufactured from ionophore/plasticizer and optimized

specifically for surfactant detection. The measurement is between the potential interactions with an ion carrier in the membrane and the ionic surfactant in the solution. When considering the probe setup as a half cell, the Nernst equation is used to relate the electrical potential with the concentration of the analyte or surfactant. This relation is the following,

$$E = E_0 + s \times \ln\left(\frac{C_{ox}}{C_{red}}\right), \quad (9)$$

where E is the cell potential (or electromotive force), E_0 is the standard cell potential (a parameter of the probe), C_{ox} is the concentration of the oxidizing agent (or anionic surfactant), and C_{red} is the concentration of the reducing agent (titrant, or hyamine). The parameters, s and E_0, are the electrode slope and standard cell potential, both properties of the probe.

In order to provide a conversion from the endpoint calculated as a measurement of the electrical potential, E, and the volume of titrant mixed with the solution, in mL, the following equation is used,

$$w_{surfactant} = \frac{V_{EP1} \times 100 \times M_S \times C_t}{m_s}, \quad (10)$$

where $w_{surfactant}$ is the surfactant concentration (wt.%), V_{EP1} is mL titrant consumed to reach the endpoint, M_s is the molecular weight of the surfactant in g/mol, c_t is the concentration of the titrant (hyamine) in mol/L, and m_s is the weight of the sample in grams. (Selig, 1980)

Chapter 3: Experimental Procedure

The goal of this work is to observe the effect of iron bearing minerals on surfactant adsorption and required the fabrication of synthetic sandstone cores with varying amounts of iron–bearing clays. This was done as an alternative to using pre-existing core samples from outcrops or reservoirs that contain iron–bearing clays where comparing the results from several corefloods can be suspect. Ideally, the fabrication of cores with similar properties would eliminate the potential that the results may be affected by varying porosity, permeability, and heterogeneity of natural sandstone cores. After fabricating the synthetic sandstone cores, the core was reduced and saturated with brine prior to an injection of a surfactant slug. The effluent was collected and analyzed using titration, potentiometric auto-titration, and HPLC equipment.

3.1: Fabrication of Synthetic Sandstone Cores

The fabrication of the synthetic sandstone cores required several precautions to ensure a homogeneous core. The procedure also served to ensure the set of cores had similar flow parameters of porosity and permeability. The steps involved in the core creation were: 1) selection and preparation of sandstone core components, 2) mixing and raining the sand, 3) freezing and trimming, and 4) loading the core into the coreholder.

3.1.1: Selection and Preparation of Sandstone Core Components

Each core used for this project consisted of silica (quartz) sand and clay, either siderite or illite. To maintain constant core parameters and limit channeling effects, a narrow range of sand particle diameters was selected. A relatively (compared to unconsolidated sand and sandstone reservoirs) large particle diameter was used, between

143 μm and 172 μm, or an 80-100 mesh sieve. The siderite and illite were crushed and ground with a burr mill, then sieved to match the particle size of the silica sand. Using a narrow size range leads to a closely-packed structure (either hexagonal close packing or face-centered cubic), and using the same size range for both sand and clay ensures that a clay particle simply replaces a sand particle in the structure.

3.1.2: Packing the Sand

The 5 synthetic cores made for the experiments consisted of silica sand and clay, the amount of clay includes 0, 2.5, 5, 10 wt% siderite and 10 wt% illite. Before packing, the mixtures were prepared by weighing the ground and sieved clay and adding the corresponding weight of silica sand into a container and agitated.

To prepare sandstone cores of consistent dimensions, a Kapton® sleeve was used to receive the sand/clay mixture. Note that, when sand is poured directly into a container from a funnel, heterogeneity can be observed due to the tendency of larger particles to bounce toward the outer walls of the container, leaving smaller particles in the center. In addition, starting/stopping leads to layering since the vibration used to achieve a close packing can also cause larger particles to rise while the packing is still loose—sometimes called the "cereal box effect". This can be seen in **Figure 11**; the upper photograph was taken after pouring a sand/clay mixture directly into a container, while the lower photograph shows the same sand prepared by distributing through a series of 5 screens while vibrating the container during packing without pause in the process.

Figure 11: a) 5% siderite sand mixture poured directly into a container (top), and b) 5% siderite poured with the distribution apparatus while vibrating the container.

To achieve a uniform packing, an apparatus was used that distributes the particles as they pass through a series of screens where the sand 'rains' into the receiving Kapton® sleeve evenly distributed across the cross–sectional area and packing the core without stopping eliminates any layering effects. **Figure 12** shows the schematic of this apparatus.

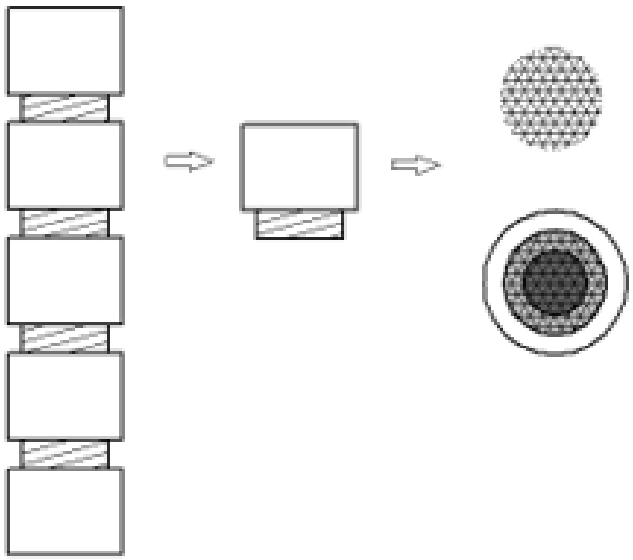

Figure 12: Schematic of distribution apparatus to prevent layering

To ensure a close packing, a vibrating platform was constructed. The platform allows for the sand to be poured through the distribution apparatus and into the Kapton® sleeve while simultaneously being slightly shaken to allow for sand re-positioning within the sleeve. A photograph of this platform is shown below as **Figure 13**.

Figure 13: Setup to distribute sand being rained into a Kapton® sleeve and shaking platform

The platform shakes due to a small motor with an eccentrically-weighted pulley attached to the drive shaft. The sand is poured from a separatory funnel that is not subject to the vibration from the motor. The stop-cock of the separatory funnel also allows for adjustment of the speed of sand raining into the Kapton® sleeve.

3.1.3: Freezing and Trimming the Core

In order to load the unconsolidated pack into a core holder, the cores were solidified by adding enough moisture to allow freezing using liquid nitrogen and then trimmed to consistent length. To achieve this, the Kapton® sleeve containing the sand mixture is immersed into a container of de-ionized water and allowed to drain so only interstitial water remains (*aka,* field capacity).

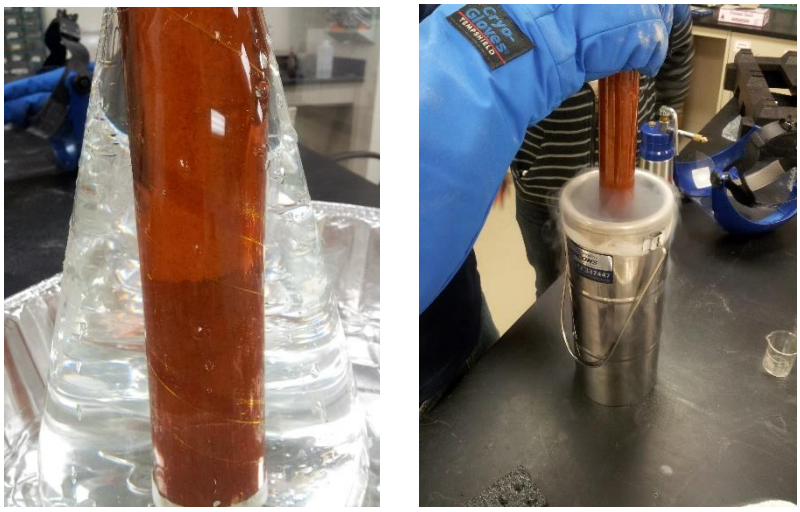

Figure 14: Once the water is drained from the unconsolidated sand pack and is at field capacity (left), the Kapton® sleeve is solidified using liquid nitrogen (right).

Figure 14 shows several photographs of this process. Draining most of the water is necessary to prevent the core from being damaged as water expands during the freezing process. Slowly, the Kapton® sleeve and sand mixture is lowered into a container of liquid nitrogen freezing the unconsolidated sand into a solid core. The Kapton® sleeve is peeled away and the solid core can then be trimmed to a specific length required by experimental standards. An image of a solid core is shown below as **Figure 15**.

Figure 15: 2.5% siderite synthetic sandstone core shortly after liquid nitrogen bath

3.1.4: Loading the Core

After the core has been prepared and frozen, it can be loaded into a rubber Viton sleeve and then placed within the metal sleeve of the Vinci® stainless steel core holder. The diagram for the core holder is shown below as **Figure 16**.

3.2: Coreflood Procedure

The coreflood was performed with equipment listed in **Table 3** and **Table 4**. The experiment injected fluids loaded into accumulators through syringe pumps. The process diagram of the experimental set-up is shown below in **Figure 17**.

The 260–mL capacity syringe pump was used for the injected fluids (reducing agent, brine, and surfactant). The 100–mL capacity syringe pump was used to inject mineral oil into the core holder to provide confining pressure on the core.

Figure 16: A photograph of the coreholder in the vertical position set–up with attached lines

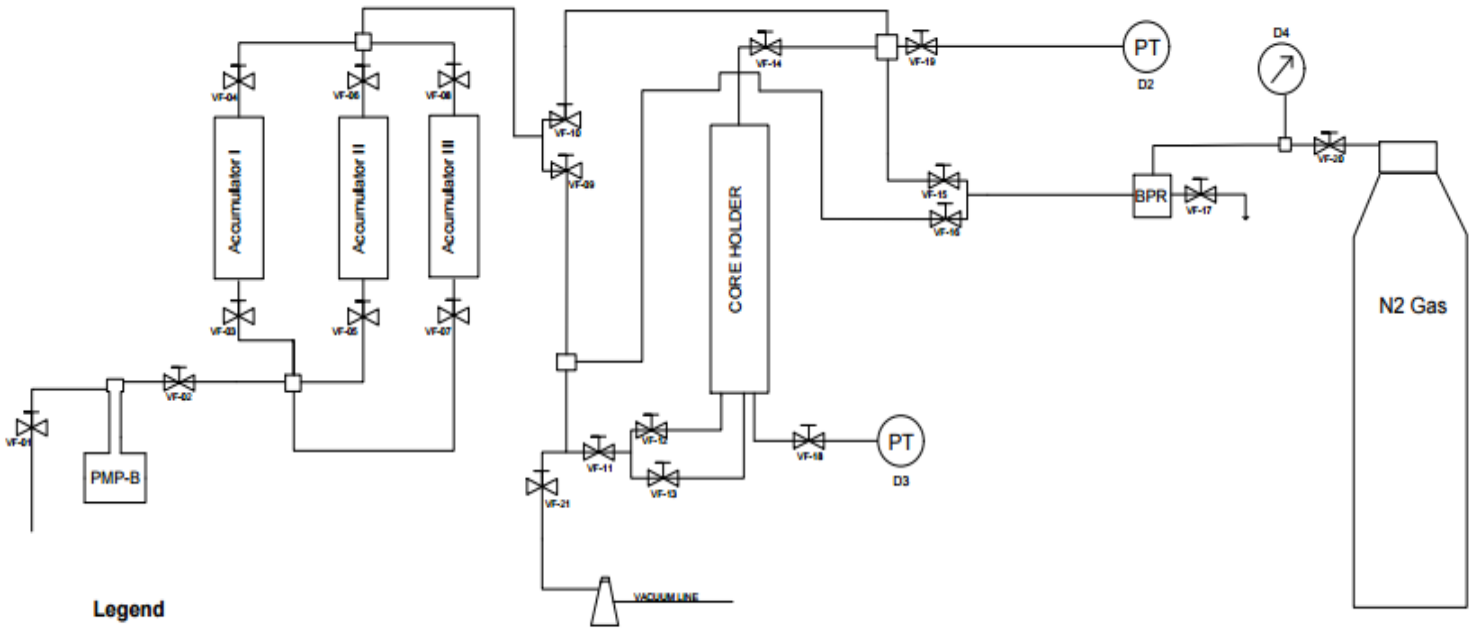

Legend

Tubing: Stainless Steel. OD: $\frac{1}{8}$" ID: 0.06" Brand: HiP.
VF : Core Flooding System Valves. Hand Operated. Maximum Pressure: 15,000 psi. Brand: HiP.
Accumulator I: Floating Piston Accumulator.Stainless Steel. Maximum Pressure: 10,000 psi. Brand: Vinci Technologies.
Accumulator II: Floating Piston Accumulator. Stainless Steel. Maximum Pressure: 10,000 psi. Brand: Vinci Technlogies.
Accumulator III: Floating Piston Accumulator. Hastelloy. Maximum Pressure: 10,000 psi. Brand: Vinci Technlogies.
Core Holder: Hydrostatic Core Holder. Model: H05-016. Core Length: 1"-12". Core Diameter: 1.5'. Hastelloy. Brand: Vinci Technologies.
BPR: Back Pressure Regulator. Model: C06-003-1. Brand: Vinci Technologies.
PMP-B: Syringe Pump B. Model 260D. Brand: Teledyne Isco.
D2, D3: Pressure Transducers outlet and inlet.
D4: Back Pressure Gauge.

Figure 17: Process Diagram – Injection and vacuum lines for coreflooding experiment

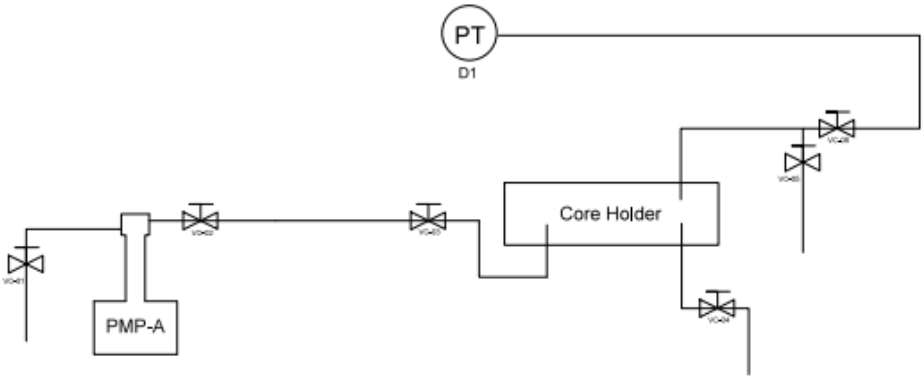

Legend

Tubing: Stainless Steel. OD: $\frac{1}{8}$ " ID: 0.06" Brand: HiP.
: Confining System Valves. Hand Operated. Maximum Pressure: 15,000 psi. Brand: HiP.
Core Holder: Hydrostatic Core Holder. Model: H05-016. Core Length: 1"-12". Core Diameter: 1.5". Hastelloy. Brand: Vinci Technologies.
PMP-A: Syringe Pump A. Model 100DX. Brand: Teledyne Isco.
D1: Pressure Transducer.

Figure 18: Confining pressure process diagram

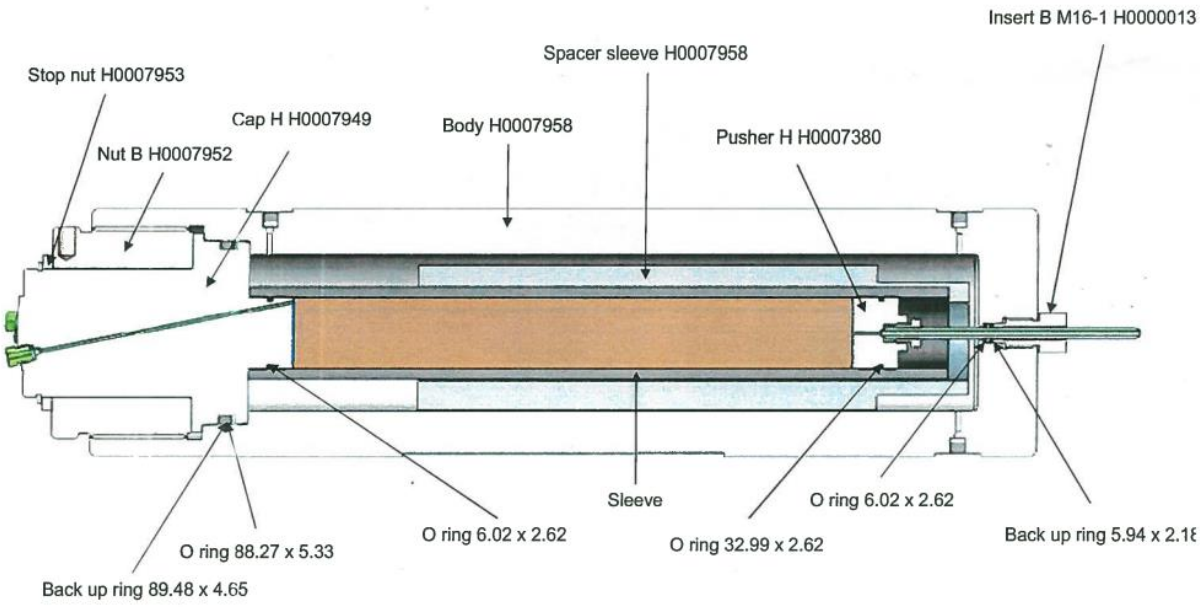

Figure 19: Detailed drawing of core holder used in experiments. Source: Vinci® Coreholder Guide and Manual.

3.2.1: Drying and De-Oxygenating the Core

After the core is loaded into the core holder and the lines are attached, nitrogen gas is allowed to flow through the system at a low flow rate in order to remove moisture from the core. The oven that houses the core holder is also set to a moderately warm temperature (150°F) to assist in the melting and drying of the solid core. Then, the nitrogen flow rate is stopped and both inlet and outlet lines are closed. A vacuum line is attached and gas is removed from the system for approximately 12 hours. It is important to remove any and all oxygen from the system as to not oxidize and reduced iron components of the clay.

To prevent oxygen from existing in and entering the experimental setup, care was taken to de-oxygenate fluids prior to their injection. This was done by bubbling argon gas into the accumulators. Any inert gas would tend to scavenge oxygen out of the injected fluids by way of bubbling from the bottom, but argon was selected due to it being heavier than air so that it also provides a 'blanket' above the fluid surface within the accumulator and prevents any oxygen from contacting the brine or surfactant.

3.2.2: Reducing the Iron Bearing Minerals and Pore Volume Measurement

As previously mentioned, the iron–bearing clays would exhibit adsorption behavior dependent upon the valence state of the iron, and we reduced the iron to a ferrous state that is more naturally found in oil reservoirs. To achieve these conditions, a reducing agent, sodium dithionite (or, sodium hydrosulfite) dissolved in de-ionized water was injected into the core. According to Rajapaksha *et al.* (2014), a reduction potential (Eh) of at least -400 mV has been found to adequately reduce the core completely allowing for an environment conducive to maximum surfactant adsorption. For all the

corefloods, after de-gassing the sodium dithionite solution with argon, we measured the Eh to be at least -400 mV. To ensure that the iron within the core was successfully reduced, the effluent Eh was measured until it matched the injected measurement.

The injection of sodium dithionite was also used as a means of measuring the pore volume of the core. As it was injected, the outlet line was closed and the system was pressurized to ensure that the core was fully saturated. Afterwards, the outlet was opened to drain and the procedure repeated several times. After the core was in a reduced state, the volume of the collected effluent was measured and compared to the injected volume. The difference between these values along with the dead volume measurements allowed for a calculation of pore volume.

3.2.3: Brine Flood and Permeability Measurements

To best observe the potential surfactant adsorption for an actual EOR project, a surfactant solution was injected at a specific salt concentration. Generally, surfactant solution formulations take into account the salinity of the formation brine so as to optimize the formation of microemulsion and increase the capillary number to mobilize residual oil in the reservoir. With this consideration, the experimental procedure first saturated the core with brine matching that salinity of the surfactant slug. As with the sodium dithionite, the brine was de-oxygenated with argon gas prior to injection.

To fully saturate the core, the brine was used to pressurize the core up to desired experimental conditions and to measure the single phase permeability (specific permeability). The permeability was calculated using the Darcy Equation (equation 11) and the pressure drop measured across the pack under steady-state flow rates of 5, 10,

and 15 mL/min. Darcy's Law can be re–written to solve for permeability, k (Darcy), with the following,

$$k = \frac{q}{\Delta P}\frac{\mu L}{A}, \tag{11}$$

where q is flow rate in mL/s, μ is viscosity in centipoise, L is length in centimeters, ΔP is pressure drop in Pascals, and A is area in cm^2. The flow rate vs. pressure drop was graphed at various flow rates to ensure linear behavior. The slope of the resulting line represents the combination of parameters, $\frac{kA}{\mu L}$. Once the slope is obtained, the permeability can be calculated with known dimensions of the sandpack and viscosity of the brine.

3.3: Surfactant Injection and Operating Conditions

The surfactant used in this experiment was an anionic, internal olefin sulfonate with an alkane chain length of between 15-18. The activity of the surfactant is 27.99% and the amount used in the injected solution was 1% as received (10 grams per 1 Liter of de-ionized water). The solution also contained the same salt (NaCl) content as the brine used to saturate the core at 30,000 ppm (30 grams per 1 Liter of de-ionized water). The surfactant was required to be anionic, as the positively–charged ferrous ions need a negatively–charged head group of the surfactant in order for adsorption to be prevalent.

Confining stress was chosen in order to simulate reservoir conditions. The confining pressure was set to 750 psi with a backpressure of 500 psi using a backpressure regulator. Temperature was maintained at a constant 100 degrees Fahrenheit. The surfactant injection rate was set to 0.05 mL/min, with each surfactant slug injected for 24

hours (a total injected volume of approximately 72 mL). The cores were 1.5 inches in diameter and trimmed to 12 inches in length.

3.4: Effluent Collection and Analysis

The effluent was collected in centrifugal tubes loaded onto a fraction collector. The fraction collector was set to shift to the next tube every 72 minutes, allowing for approximately a 4-mL sample to be collected in each tube. Several methods were used to measure the concentration of the collected surfactant in each sample. The first was manual titration technique with burette and a solution of methylene blue and hyamine cationic surfactant. The second was a potentiometric titration using an autotitrator with hyamine as the titrant. An electrode probe measured the potential energy in mV as the titrant was added, the final concentration calculated from a relation.

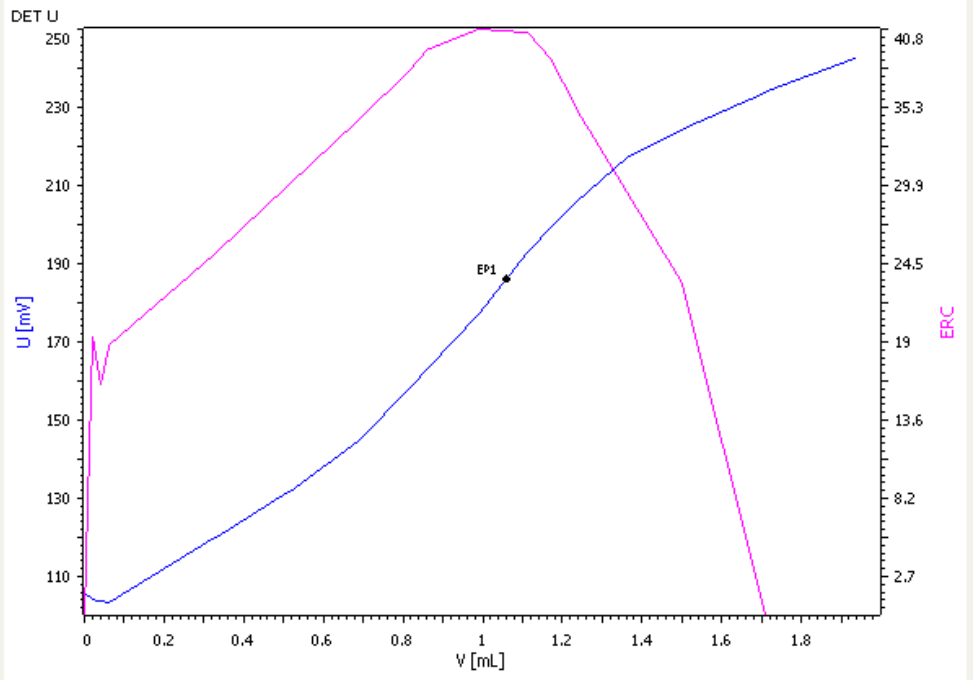

Figure 20 – Titration curve output for injected surfactant used in Experiment 4 – 5% siderite sand pack

Figure 20 is an example output titration curve. In this graph, the blue line is the measured electric potential across the probe with the endpoint designated as EP1. The second, magenta curve is the first derivative of the electric potential curve. It is a visual aid in determining the inflection point and is a max at the inflection point EP1.

In order to calculate the adsorption, the mass of the surfactant collected was subtracted from the mass of the surfactant injected. The total mass of surfactant injected was calculated by measuring the initial concentration of surfactant in the solution and multiplying by the total collected volume during the injection process. The total mass of surfactant collected was obtained by summing the mass in each sample, which were found by multiplying the concentration measurements of each effluent sample by its respective volume.

3.5: Post Experiment Core Preservation

After the experiment, the 2.5%, 5%, 10% siderite cores and the 10% illite cores were preserved. To do this, a gelatin (common food additive) mixture was prepared with deionized water and poured into the Viton sleeve containing the sand pack after being removed from the core holder. The result was a semi-solid sand pack that can be sampled and examined to compare with pre-experiment core samples that were also saved.

3.6: Materials and Equipment

The following table lists of all chemicals and compounds used in the experiment.

Table 3: Experimental materials

Material	Description
surfactant	Enordet – 0332 : IOS 15-18 Activity 27.99% : MW 350 : pH 14
sand	US Silica OK-75 : 143 – 175 micrometers
siderite	Sidco Siderite – $FeCO_3$
illite	Ward's Illite shale, 85%, Maplewood Shale – Rochester, NY
NaCl	Sigma-Aldrich Sodium chloride Lot # SLBL0434V >99.5%
KCl	Cole Parmer Reference Fill Solution, 4M
sodium dithionite	Alfa Aesar Sodium Hydrosulfite 85 +% Na2S204 : Lot #W30B038
hyamine	Titripur 1.15480.1000 Hyamine 1622 Solution : 0.004 mol/l
mineral oil	Walgreen Company Mineral Oil 0363-0210-06

The following table contains a list of equipment used and description.

Table 4: Experimental equipment used in research

Equipment	Description
core holder	Vinci® Technologies, Model H05-016 : Hydrostatic, Hastelloy:
syringe pump (injection)	Teledyne Isco Syringe Pump : Model 266DX
syringe pump (confining)	Teledyne Isco Syringe Pump : Model 100DX
pressure transducer – inlet	Rosemount Smart Family Transducer, rated to 4,000 psia
pressure transducer – outlet	Rosemount Smart Family Transducer, rated to 10,000 psi
tubing	HiP : Stainless Steel OD 1/8" ID 0.06"
valves	HiP : Stainless Steel Hand Operated : rated to 15,000 psi
backpressure regulator	Vinci® Technologies : Model CD6-003-1
balance	Mettler PE 3600
viton sleeve	Vinci® Technologies : Viton rubber sleeve
accumulators	Vinci® Technologies : stainless steel floating piston : maximum pressure 10,000 psi
fractional collector	Teledyne ISCO Fractional Collector
auto-titrator	Metrohm 888 Titrando with 801 stirrer
surfactant probe	Van London Co : Model SUR1502
ORP probe	Oakton Waterproof ORPTestr10 : Double Junction
liquid nitrogen	Matheson, High Purity
nitrogen gas	Matheson, Ultra High Purity
argon gas	Matheson, Ultra High Purity
backpressure gauge	3D Instruments 10,000 psi gauge
confining pressure gauge	Stewarts USA 20,000 psi gauge
oven	Blue Electric Model POM-1403CX : Rated to 400 F

Chapter 4: Results and Discussion

The set of experiments for this study includes sand packs composed of varying amounts of silica sand and siderite or illite. Ion Pairing Chromatography analysis was performed on the siderite and illite clays to determine the weight percentage of relevant cations within them. The results are shown in **Table 5**.

Table 5: General experiment description for this work

Experiment	Composition
1	100% silica sand
2	97.5% silica sand, 2.5% siderite
3	95% silica sand, 5% siderite
4	90% silica sand, 10% siderite
5	90% silica sand, 10% illite

Table 6: Ion pairing chromatography analysis of illite and siderite samples

Cation(wt.%)	Siderite	Illite
Al	1.14	7.95
Ca	0.15	0.52
Fe	34.73	2.68
K	0.12	4.51
Mg	0.11	1.13

4.1: Sand pack Cores

Each of the synthetic sand pack cores were made according to the procedure outlined in Chapter 3. Photos of each core are shown below. The photos are shown with measuring tape to indicate the length of the cores after they have been trimmed and prepared to be placed in to the core holder. **Figure 21** shows the core with only white silica sand. As the weight percentage of clay increases in each of the cores, **Figures 22-25** show the color shade grow darker (red for siderite clay and green for illite).

Each sand pack was 1.5-inch diameter using a Kapton® sleeve during the fabrication. The frozen sand packs were trimmed to be 12-inches in length, with some slight variation due to cutting inconsistency. The weight of the pack was measured after sand distribution in the Kapton® sleeve and prior to freezing with liquid nitrogen. Since exact component masses are unknown after the freezing and cutting process, they are estimated based on a bulk density measured of the pack and weight percentages of each component in the bulk mixture. Properties of each sand pack are contained in the **Table 7**.

Figure 21: 100% silica sand pack

Figure 22: 2.5% siderite sand pack

Figure 23: 5% siderite sand pack

Figure 24: 10% siderite sand pack

Figure 25: 10% illite sand pack

Table 7: Properties of each sand pack

Experiment	Length (in.)	Bulk Density (g/cm^3)	Bulk Volume (cm^3)	Mass of Siderite (g)	Mass of Silica (g)	Mass of Illite (g)
1	12.0	1.633	347.5	0	567.5	0
2	12.0	1.635	347.5	13.9	554.2	0
3	12.0	1.636	347.5	28.4	540.1	0
4	11.9	1.675	344.3	57.7	519.0	0
			342.6	0	516.4	57.4
5	11.8	1.662	330.6*	0	494.5*	54.9*

*During experiment, some volume of sand was produced and collected at the output. This was subtracted from the bulk volume to correct the subsequent analysis and calculations.

In **Table 7**, experiment 5 is shown with two values. During the experimental determination of porosity, roughly 12 mL of sand were collected in the effluent and thus was removed from the resulting calculations.

4.2: Porosity and Sand Pack Iron Reduction

The results of the reduction measurements, pore volumes measured, and porosity calculated are included in **Table 8**. The reduction measurements are shown in columns labeled "Eh" to report the reduction potential value for the fluid at injection and then also after the fluid was collected at the outlet. This value was obtained using an ORP meter

(oxidation/reduction potential). The porosity calculations for each experiment showed a relative consistency, with a slight decreasing trend as clays were added. In experiment 1, the core was flooded using sodium dithionite for consistency, but the Eh was not measured as the sand contained no iron bearing minerals that required reduction.

Table 8: ORP data and porosity measurements

Experiment	Eh (mV), Injected	Eh (mV), Collected	Pore Volume (mL)	Porosity (%)
1	--	--	110.4	31.7
2	-537	-534	90.4	26.0
3	-540	-541	93.0	26.8
4	-550	-550	100.5	29.2
5	-502	-494	81.3	24.4

There was an error in the porosity procedure for Experiment 4, where a leak above the accumulator prevented accurate measurement of the injected volume. As a result, an estimate was made after determining the porosity of a piece of core that was left from the core trimming process. This is the value reported in **Table 8**. In general, it appears that porosity remained unaffected from the introduction of clays minerals, as all of the porosities ranged between 24% and 31%.

4.3: Permeability

The permeability calculations were performed from pressure measurements made for brine flow at rates between 5 mL/min and 20 mL/min. Unlike the porosity, there appeared to be a trend of decreasing permeability as the weight percent of siderite

increased in each of the sand packs. A notable permeability was measured for a high weight percent of illite, which had a high permeability similar to the simple silica core. **Table 9** reports the permeability and the data used for the calculations.

Table 9: Permeability calculation data

Experiment	ΔP (Pa) @ q = 5 mL/min	ΔP (Pa) @ q = 10 mL/min	ΔP (Pa) @q = 15 mL/min	ΔP (Pa) @ q = 20 mL/min	Slope ($\frac{k\mu L}{A}$)	Viscosity (cP)	Permeability (Darcy)
1	0.110892	0.124285	0.138519	--	6.03	1.05	16.9
2	0.01215	0.029457	0.043075	--	5.36	1.05	15.1
3	--	0.075531	0.090221	0.120668	3.27	1.05	10.0
4	0.033257	0.051647	0.08567	--	3.09	1.05	8.6
5	0.029103	0.044643	0.054649	--	6.78	1.05	18.8

These data are also plotted in **Figure 26 - Figure 30** with the linear trends and curve fit. The overall permeability trend as a function of increasing weight percentage of siderite is visualized in a graph in **Figure 31**.

4.3: Adsorption

The surfactant adsorption was calculated using the surfactant concentration measured in the effluent of the flood. To obtain the mass of surfactant retained in the sand pack, the sum of the calculated mass of surfactant in each sample was subtracted by the total mass of surfactant injected. The surfactant flood for the core containing only

silica was used as a basis to determine the adsorption due to sand versus the clay. **Figure 32 - Figure 36** show the concentration history for all the surfactant floods. The concentration is shown as a ratio between the measured concentration and the initial concentration (C/C_0 - dimensionless) in these graphs. **Table 10** summarizes the adsorption measurements.

Table 10: Adsorption Data for the surfactant floods

Experiment	Percent Retained (%)	Overall Retention (g)	Adsorption due to silica (g)	Adsorption due to clay (g)	Adsorption with respect to iron (mg Surf/g Fe)
1	11.04	0.020	0.020	--	--
2	15.55	0.037	0.0195	0.0175	3.6
3	26.8	0.054	0.0190	0.0350	3.6
4	--	--	--	--	--
5	12.3	0.025	0.0176	0.0074	4.9

In experiment 5, illite was used instead of siderite. The overall adsorption was due mostly to the silica within the core, with a small degree of adsorption due to the illite clay. Since the illite has a lower iron content compared to siderite, a lower degree of adsorption based on clay content is reasonable. When the adsorption is computed based on iron content, the adsorption for all the experiments are between 3.6 and 4.9 mg/g of iron, with the adsorption for the illite experiment being higher than that of the siderite based on iron content.

In Experiment 4, very little to no surfactant was detected in the effluent. This result was not expected, especially when the previous experiments (1, 2 and 3) resulted in consistent values for surfactant adsorption based on iron content. It is possible that the surfactant may have been present, but the concentration was too low to adequately measure with potentiometric titration. In order to obtain meaningful data from this experiment, a second attempt was made using the same core and a constant injection of surfactant that should result in a smooth increase in concentration (often called a 'S' curve), however, the concentration increase fluctuated until the effluent concentration reached that of the injected surfactant concentration (see **Figure 36**). This may be due to layering of surfactant micelles on the active sites of the clay minerals, as shown in **Figure 10**, and subsequent shearing off surfactant molecules at intermittent periods. This layering and subsequent shearing effect may explain the fluctuation at the peak of the concentration history profiles in **Figures 33-35** (Experiments 2, 3, and 5).

4.4: First Moment Analysis

The method of moments was used to determine the retention time of the fluid travelling through the porous media. When partitioning occurs, a delay in the production of the injected fluid is observed. During injection of fluids that are subject to adsorption on the medium, this partitioning can also be observed as a slight degree of retardation. The below table shows the results of the first moment analysis.

Table 11: First temporal moment for the series of surfactant floods

Experiment	First Moment (PV)	Retardation Factor ($\frac{\overline{V_2}}{\overline{V_1}}$)
1	1.02	1
2	1.22	1.19
3	1.38	1.35
4	--	--
5	1.84	1.80

A plot shown in **Figure 37** of the first moment as a function of the weight percentage of clay in the sand pack shows a linear trend for the experiments containing siderite. The delay for the illite experiment falls very near this trend line as well. This indicates that the partitioning effect of the surfactant onto clay surfaces is proportional to the amount of clay present.

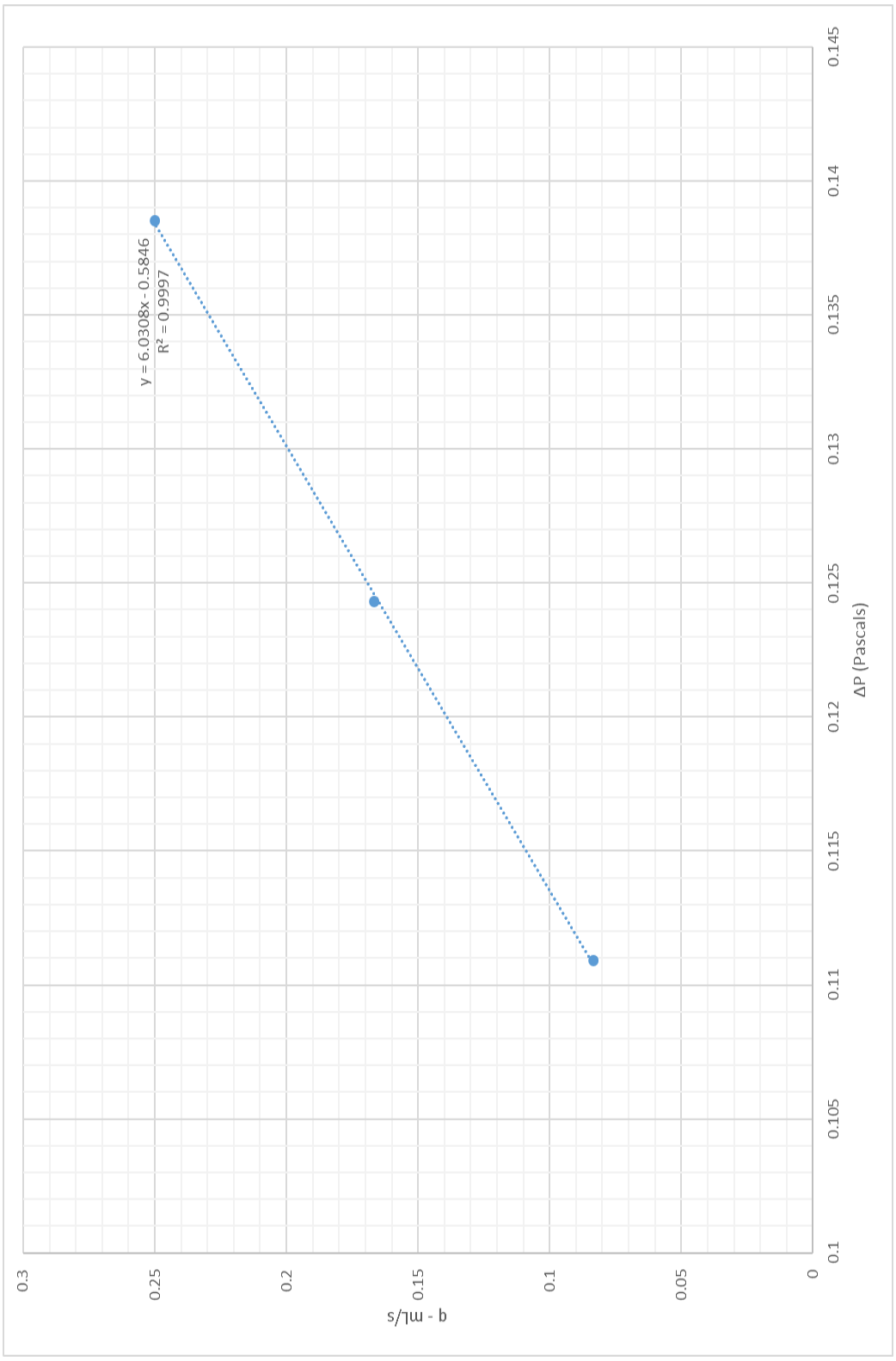

Figure 26: Pressure drop at steady-state flow rate used to compute permeability for 100% silica sand pack

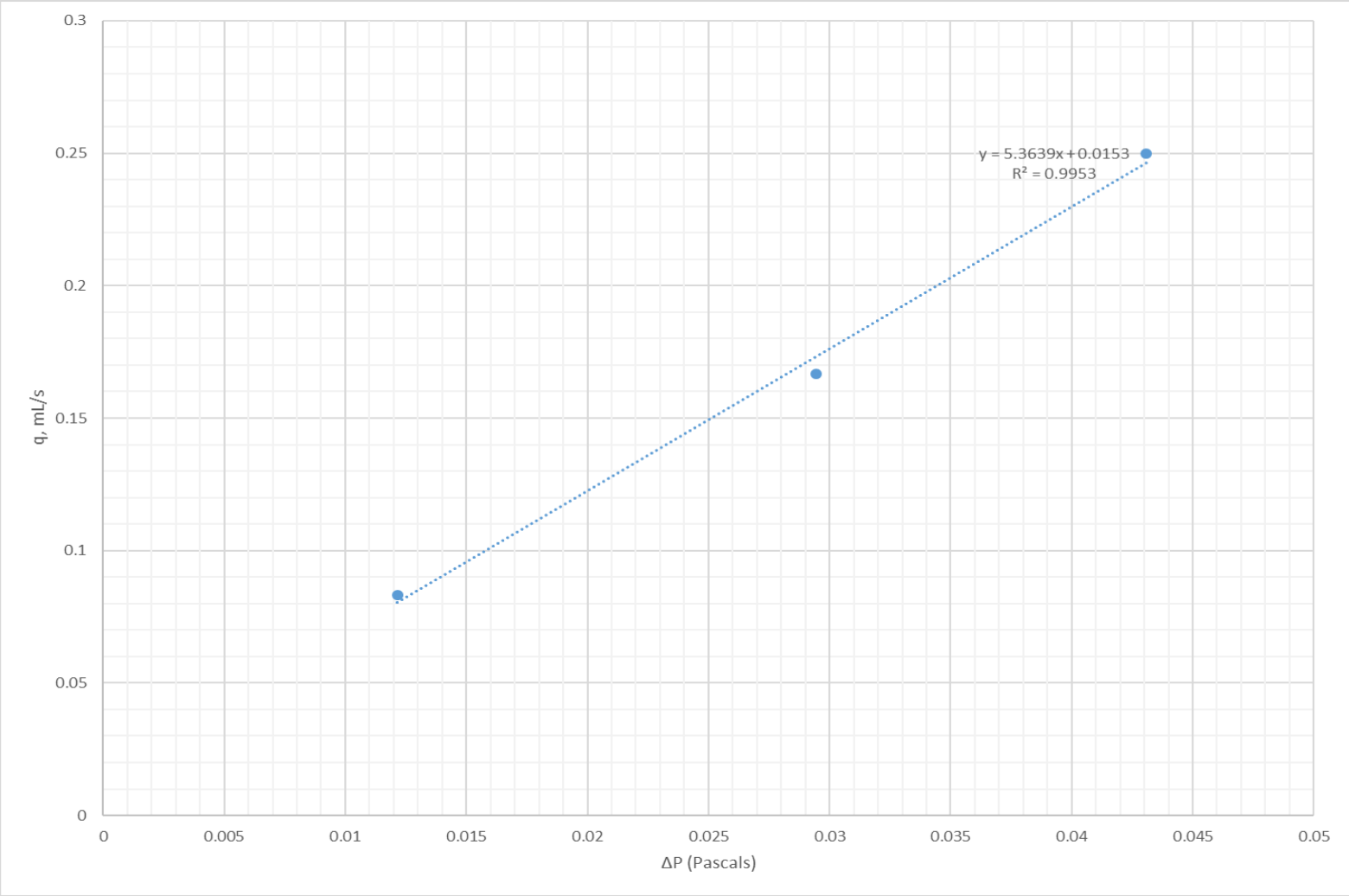

Figure 27: Pressure drop at steady-state flow rate used to compute permeability for 2.5% siderite pack

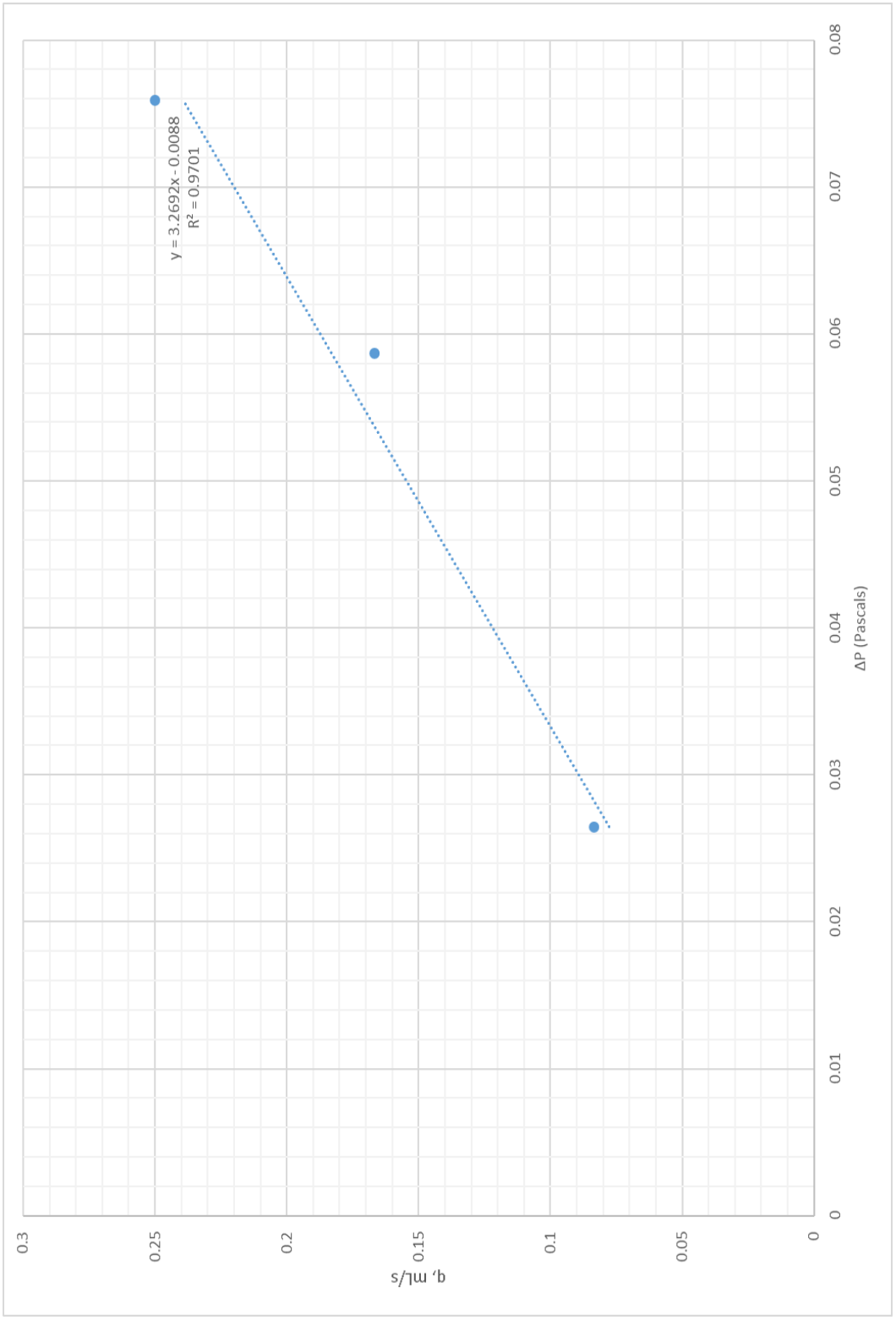

Figure 28: Pressure drop at steady-state flow rate used to compute permeability for 5% siderite pack

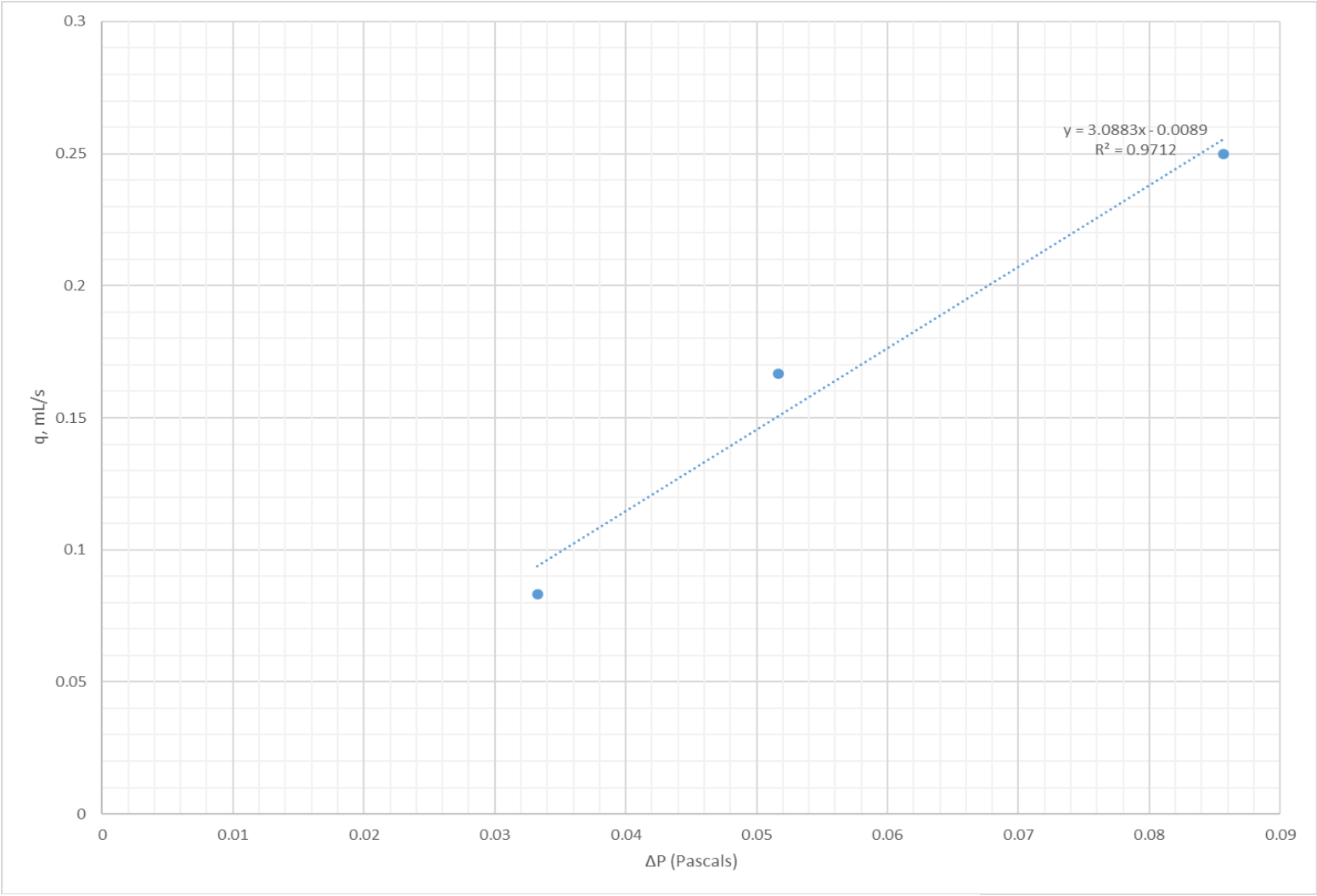

Figure 29: Pressure drop at steady-state flow rate used to compute permeability for 10% siderite pack

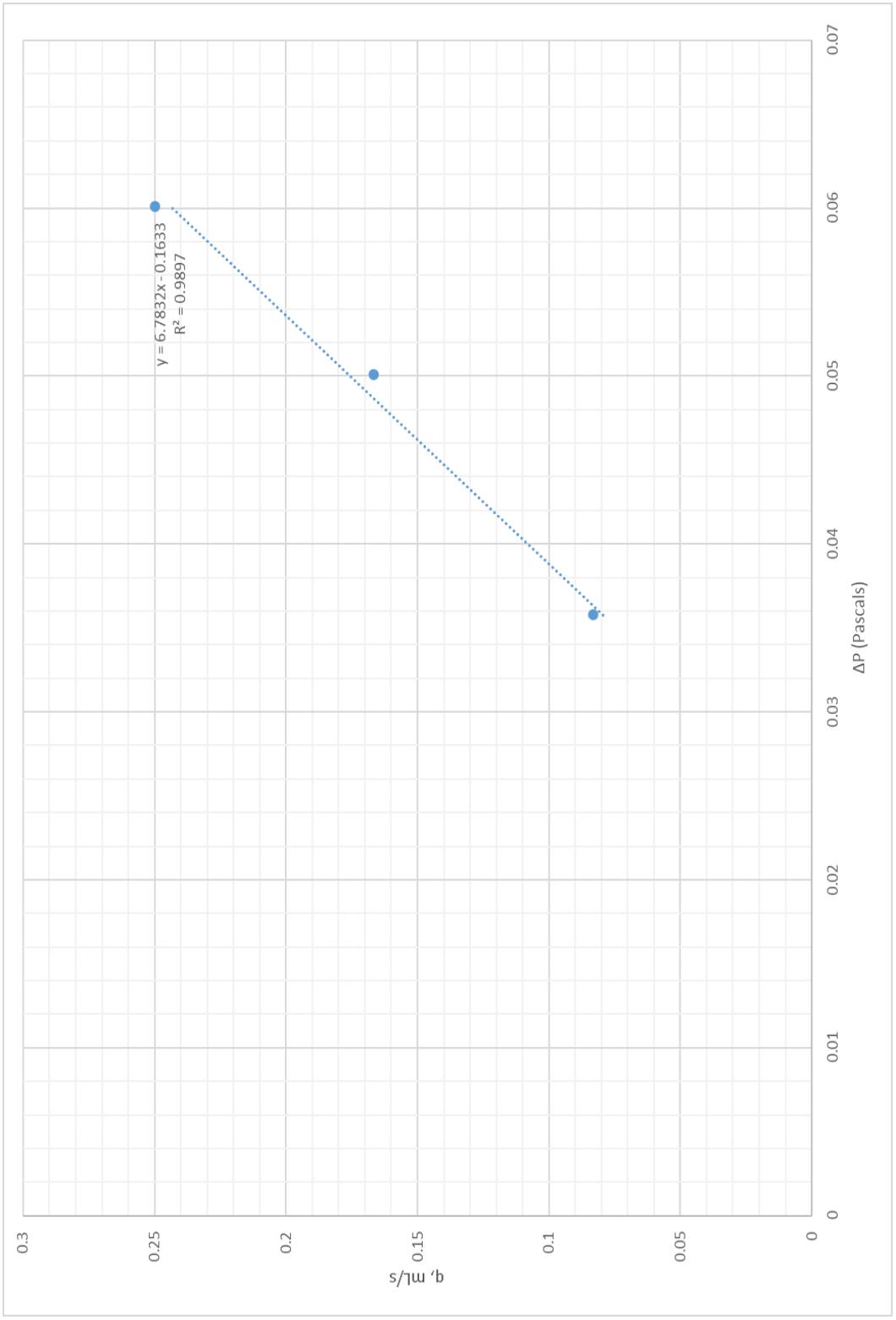

Figure 30: Pressure drop at steady-state flow rate used to compute permeability for 10% illite pack

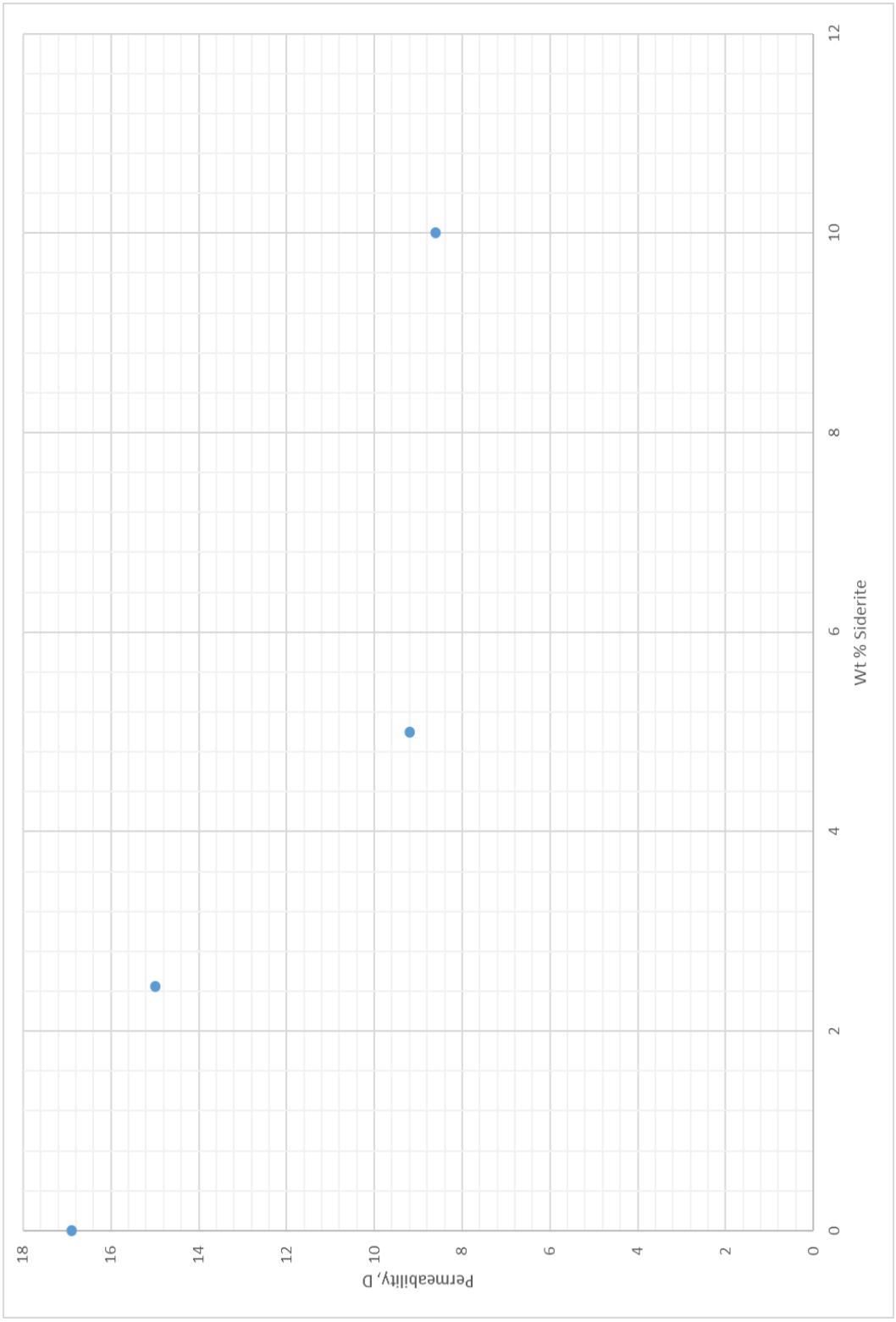

Figure 31: Permeability trend with increasing siderite content

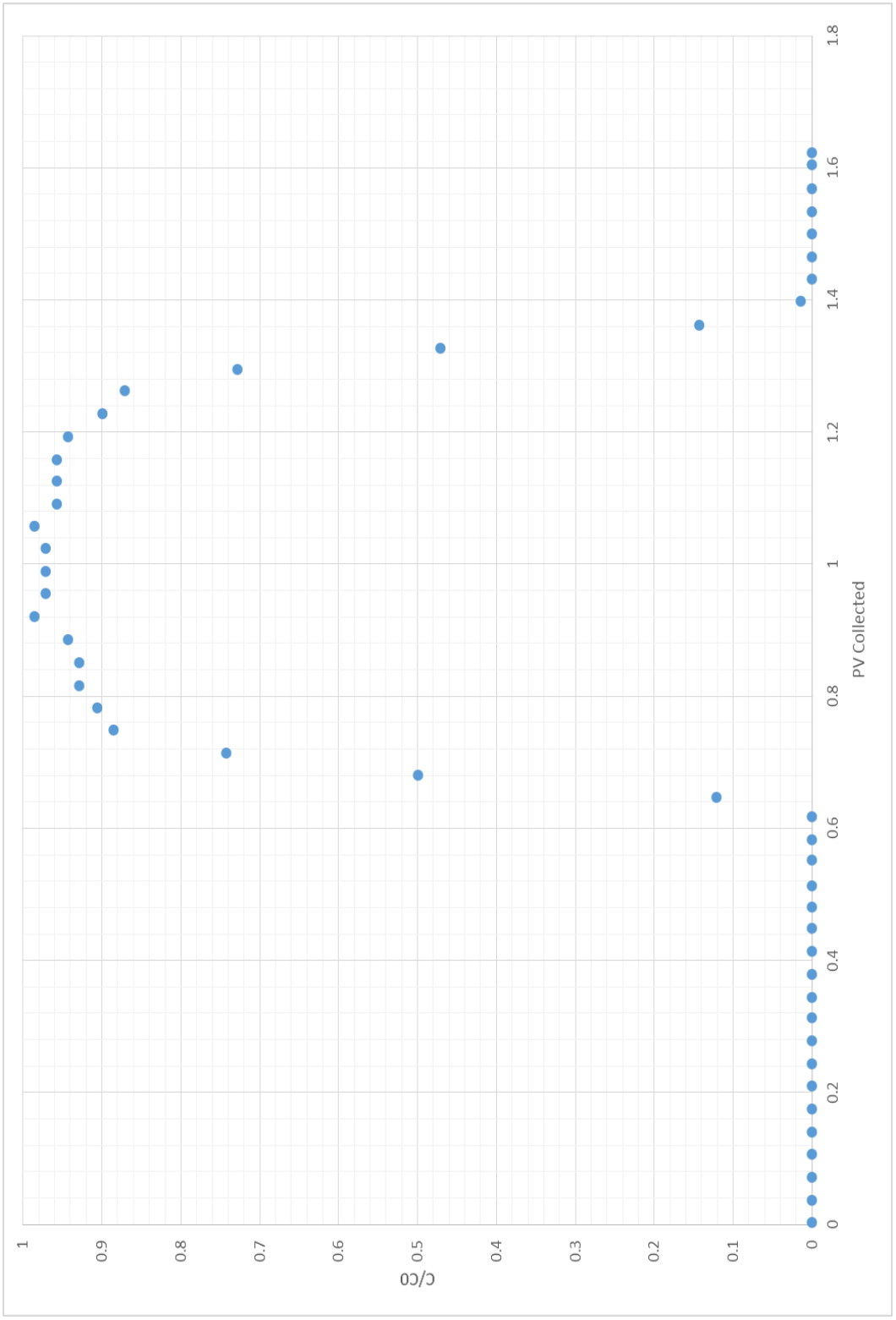

Figure 32: Concentration of surfactant versus pore volumes collected, 100% silica

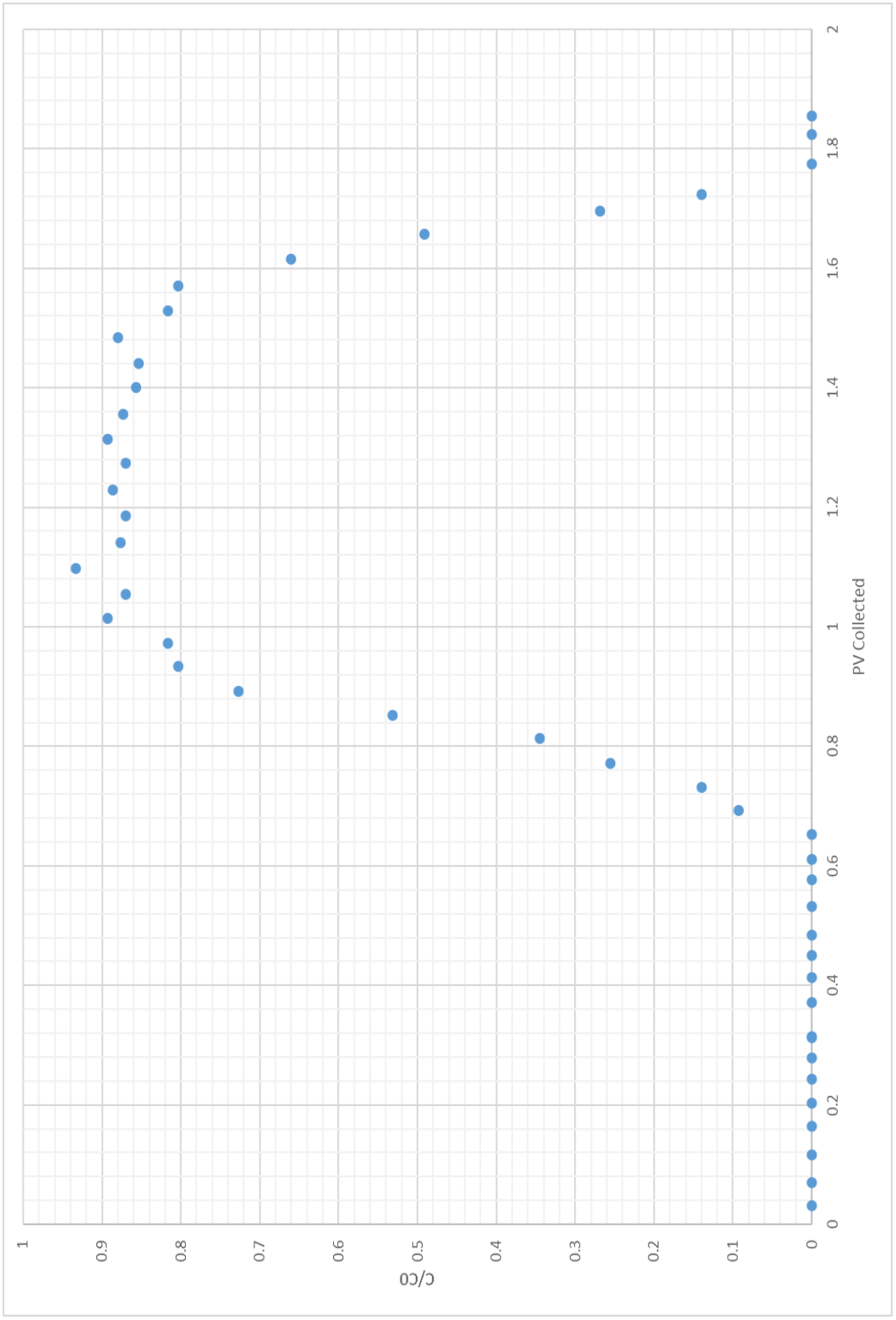

Figure 33: Concentration of surfactant versus pore volumes collected, 2.5% siderite

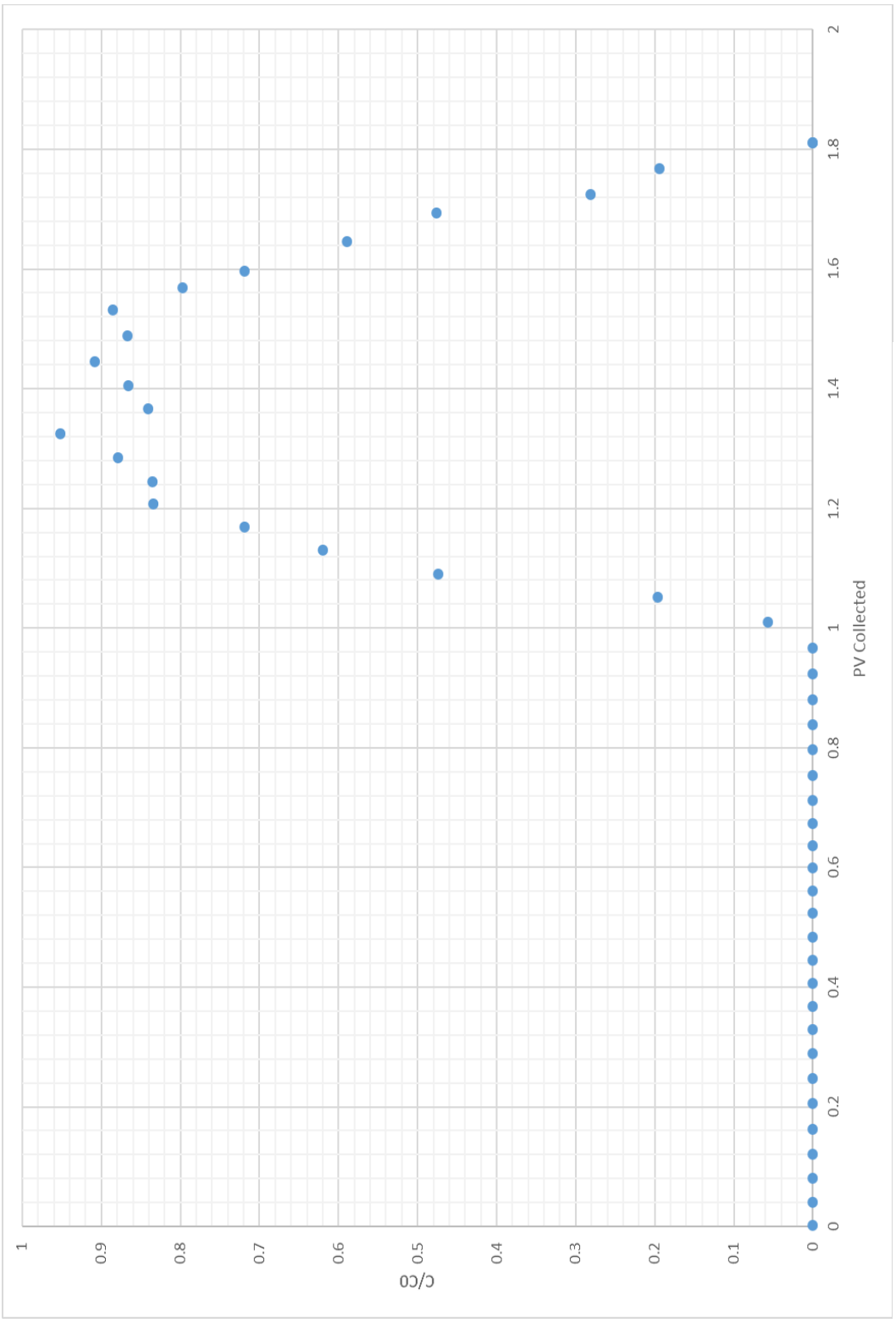

Figure 34: Concentration of surfactant versus pore volumes collected, 5% siderite

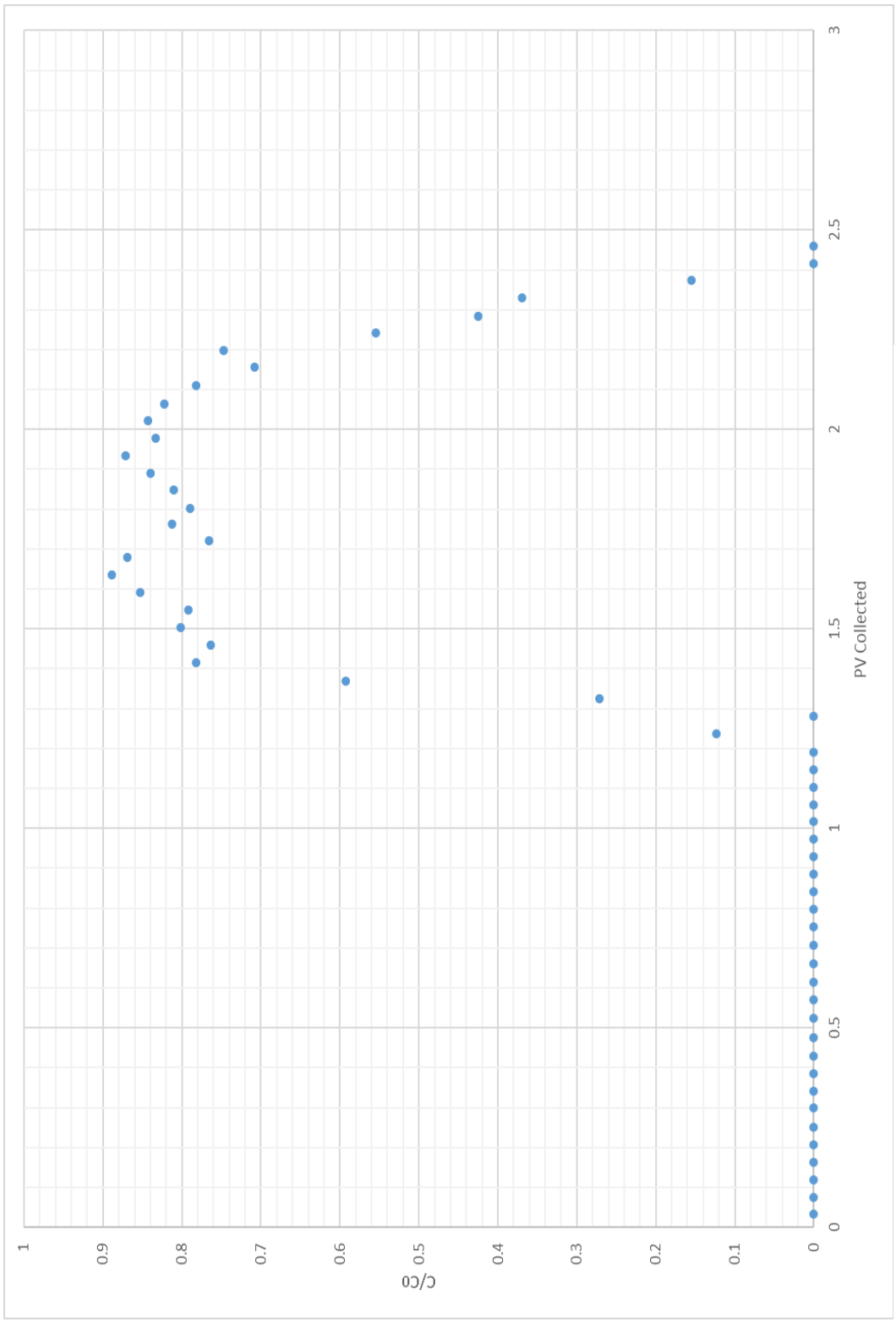

Figure 35: Concentration of surfactant versus pore volumes collected, 10% illite

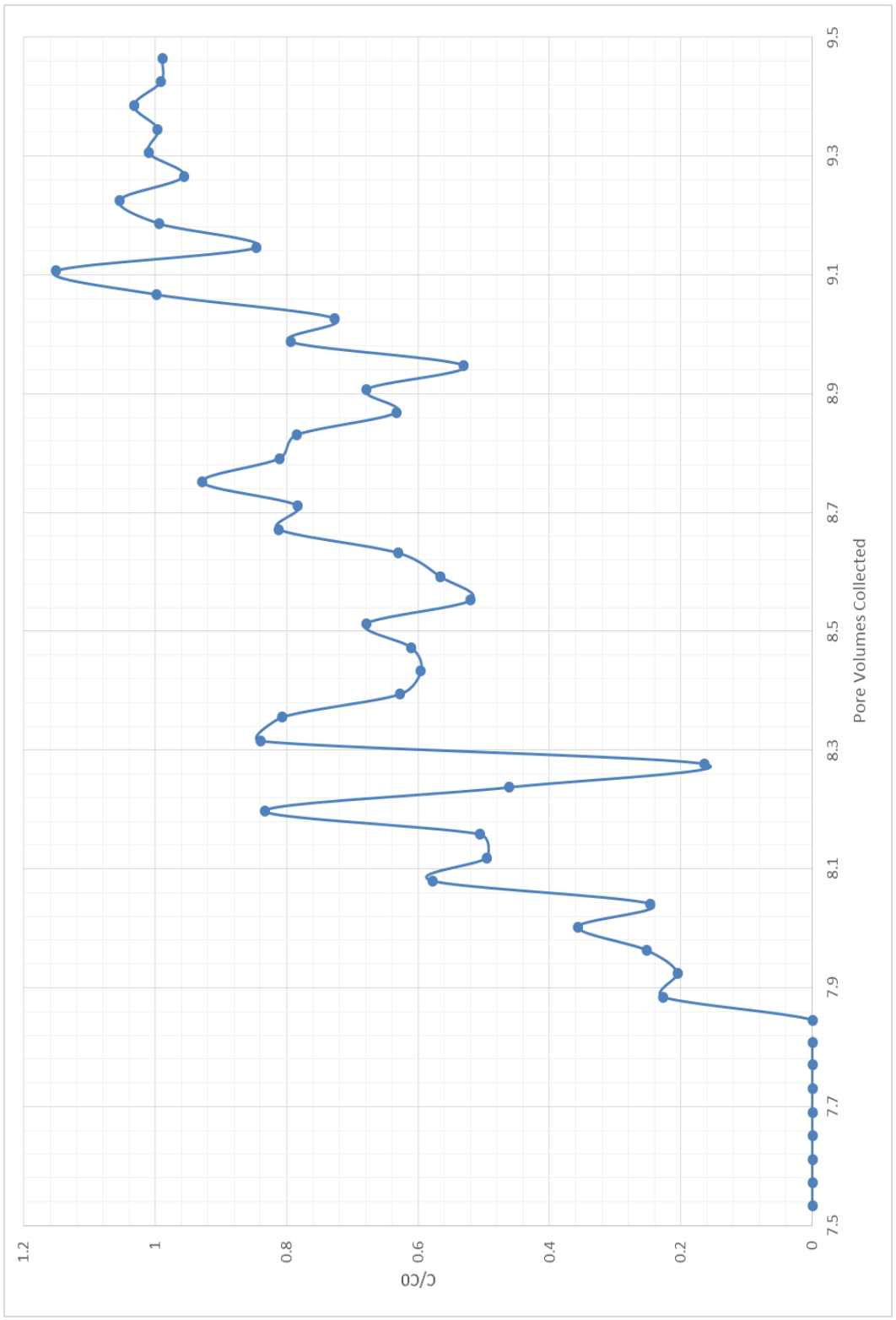

Figure 36: Surfactant concentration history for synthetic core containing 10% siderite

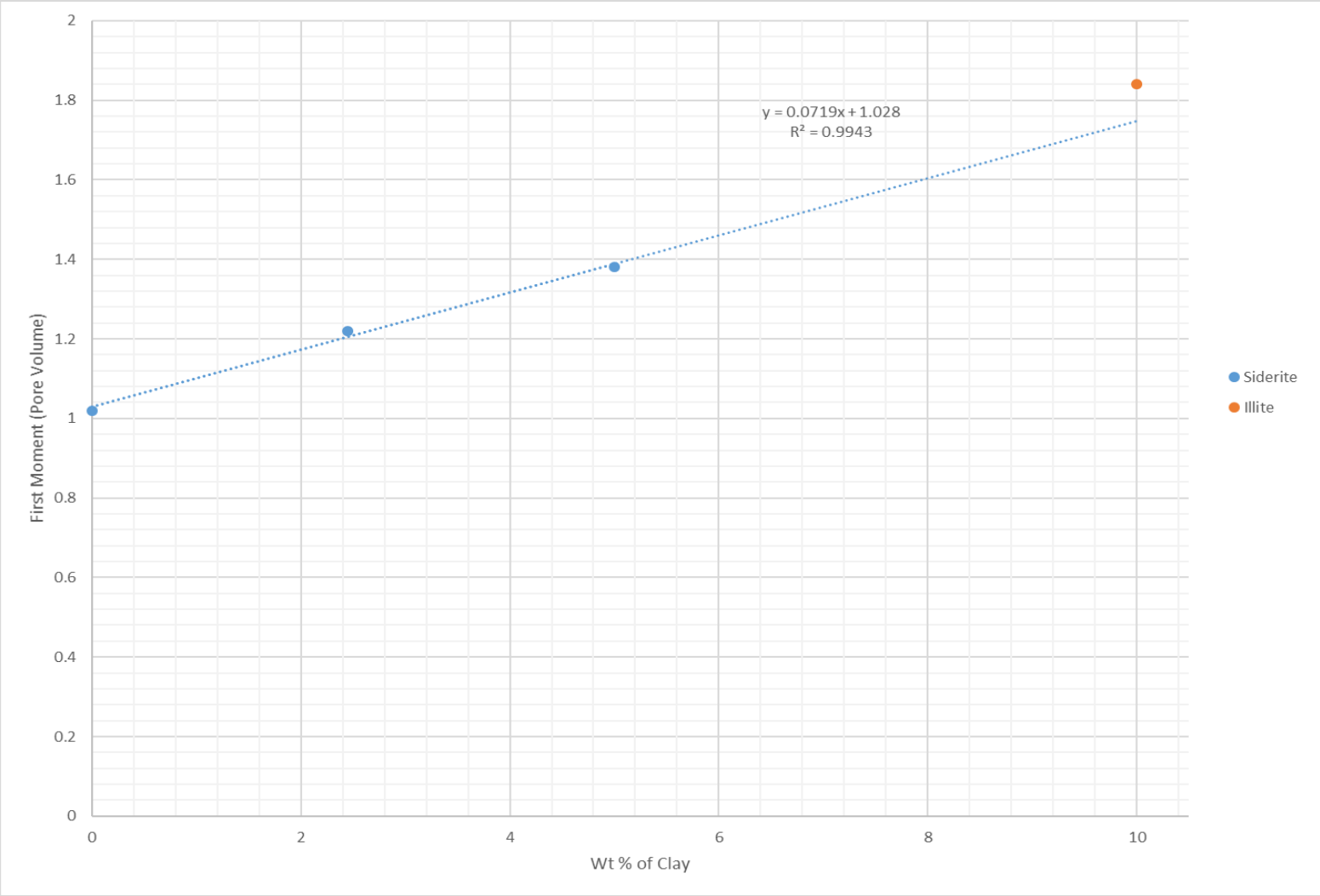

Figure 37: First moment versus weight percent of clay and subsequent trendline

Chapter 5: Conclusions

A series of 5 experiments were performed to observe the effect that iron–bearing clays have on surfactant retention within synthetic sand packs. Sand packs with varying amounts of siderite or illite were fabricated. It was concluded that the addition of clays had little effect on porosity using the fabrication approach, but a higher clay content correlated with a lower permeability. This is likely due to clay surface charge effects known to increase the amount of bound water and in particular the strength of the surface charge; higher amounts of siderite (with a higher Fe^{2+} ion content) corresponded with decreases in permeability, while higher amounts of illite (with lower iron content) had no discernible effect on permeability.

Retention of an internal olefin sulfonate surfactant (hydrocarbon length of 15-18) was approximately 3.6 mg/g–iron (ferrous) based on the experimental results that used siderite (2.5 wt.% and 5 wt.%). The sand pack containing 10 wt.% illite exhibited a slightly higher degree of retention, which could be attributed to experimental error or the presence of additional ions such as aluminum cations in the clay.

The concentration profile of the effluent was difficult to determine for the experiment conducted with the highest siderite content, 10 wt.%. This could be due to limitation of the potentiometric autotitration technique at low surfactant concentrations, or because adsorption increases dramatically at a certain point above 5% siderite by weight. In cases of sand packs with high iron content, there is evidence that surfactant micelles adsorb to the surface and to each other, with eventual shearing resulting in an erratic concentration profile in the effluent after constant surfactant injection.

The method of moments was used to calculate the retention factor for each of the core floods. There is trend of increased partitioning (adsorption/desorption) as clay content was increased, regardless of the amount of iron in the clay. The trend was linear for the series of corefloods which used siderite clay; the single coreflood using illite also appears to follow the same trend. This may indicate that the partitioning effect is more related to clay content than iron.

5.1: Future Work

For future studies, it would be important to confirm the consistency of retention due to iron content by performing more studies with varying weight content of siderite, such as 7.5% by weight. Studies using different anionic surfactant types, such as varying the hydrocarbon chain length, could also determine the overall effect that iron bearing minerals have on surfactant retention. Using surfactants that are detectable by HPLC analysis could improve our ability to detect low surfactant concentrations. More studies with illite and other iron–bearing minerals could assist in confirming that retention is correlated more with iron cations and not other metal content within the minerals. Since a layering and shearing effect may have been observed with high siderite (and high iron) content, more studies should be done at similar weight percentages to confirm this phenomenon.

References

Bantignies, Jean Louis, Christophe Cartier Dit Moulin, and Herve Dexpert (1997), "Wettability Contrasts in Kaolinite and Illite Clays: Characterization by Infrared and X-Ray Absorption Spectroscopies", *Clays and Clay Minerals*, Vol. 45-2, 184-193

Bera, Achinta, T. Kumar, Keka Ojha, and Ajay Mandal (2013), "Adsorption of surfactants on sand surface in enhanced oil recovery: Isotherms, kinetics and thermodynamic studies," *Applied Surface Science***,** 284, 87-99.

Dwarakanath, Varadarajan, Neil Deeds, and Gary A. Pope (1999), "Analysis of Partitioning Interwell Tracer Tests," *Environmental Science and Technology***,** 33, 3829-3836.

EIA (2016), "Annual Energy Outlook 2016 with projections to 2040", DOE/EIA. 0383, MT1-MT32

ElMofty, Omar (2012), "Surfactant enhanced oil recovery by wettability alteration in sandstone reservoirs," Masters Thesis, Missouri University of Science and Technology, Paper 6928.

Hirasaki, George J., Clarance A. Miller, and Maura Puerto (2011), "Recent Advances in Surfactant EOR," *SPE Journal*, December, 889-907.

Holmberg K, Jonsson B, Kronberg B, Lindman B (2002), *Surfactants and polymers in aqueous solution*, Wiley, Hoboken NJ.

Jin, Minquan (1995), “A Study of Nonaqueous Phase Liquid Characterization and Surfactant Remediation”, University of Texas at Austin PhD Dissertation, 90-108

Kamari, Arash, Mehdi Sattari, Amir H. Mohammadi, and Deresh Ramjugernath (2015), "Reliable Method for the Determination of Surfactant Retention in Porous Media during Chemical Flooding Oil Recovery", *Fuel*, 158, 122-128

Knag, Magne, Johan Sjoblom, Gisle Oye, and Egil Gulbrandsen (2004), "A quartz crystal microbalance study of the adsorption of quaternary ammonium derivatives on iron and cementite", *Colloids and Surfaces A: Physiochemical Engineering Aspects*, 250, 269-278

Knag, Magne, Tekla Tammelin, Katerina Bilkova, Leena-Sisko Johansson, Egil Gulbrandsen, and Johan Sjoblom (2006), "Adsorption of Polycation and Anionic Surfactant onto Iron Surfaces and the Inhibition of Carbon Dioxide Corrosion", *Journal of Dispersion Science and Technology*, 27, 277-292

Lake, Larry W., Russell T. Johns, William R. Rossen, and Gary A. Pope (2014), *Fundamentals of Enhanced Oil Recovery*, 84-319, Richardson TX: Society of Petroleum Engineers

Owen, Nick, and Oliver R. Inderwildi (2010), "The status of conventional world oil reserves-Hype or cause for concern?", *Energy Policy*, 38, 4743-4749

Paria, Santanu, and Kartic C. Khilar (2004), “A review on experimental studies of surfactant adsorption at the hydrophilic solid-water interface,” *Advances in Colloid and Interface Science*, 110, 75-95.

Rajapaksha, Suneth, Chris Britton, Robert I. Mcneil, Do Hoon Kim, Michael Unomah, Erandimala Kulawardana, Nadeeka Upamali, Upali P. Weerasooriya, and Gary A. Pope (2014), “Restoration of Reservoir Cores to Reservoir Condition before Chemical Flooding Tests”, *SPE Journal*, 169887-MS

Selig, S. (1980), "The potentiometric titration of surfactants and soaps using ionselective electrodes", *Fresenius Journal of Analytical Chemistry*, 300, 183-188

Sheng, James J.(2011), *Modern Chemical Enhanced Oil Recovery: Theory and Practice*, 239-349, Houston, TX: Gulf Publishing Company

Sheng, James J. (2015), “Preferred calculation formula and buoyancy effect on capillary number,” *Asia-Pacific Journal of Chemical Engineering***,** 10(3), 400-410.

Somasundaran, P., Thomas W. Healy, and D.W. Fuerstenau (1964), "Surfactant Adsorption at the Solid-Liquid Interface - Dependence of Mechanism on Chain Length", *The Journal of Physical Chemistry*, 68-12, 3562-3566

Wang, F.H.L. (1993), "Effects of Reservoir Anaerobic, Reducing Conditions on Surfactant Retention in Chemical Flooding", *SPE Reservoir Engineering*, 8-02, 108-116

Wilhite, G. Paul (1986) *Waterflooding*, 1-110, Richardson, TX: Society of Petroleum Engineers

Zhang, Rui, and P. Somasundaran (2006), "Advances in adsorption of surfactants and their mixtures at solid/solution interfaces", *Advances in Colloid and Interface Science*, 123-126, 213-229